STATIC AND DYNAMIC BEHAVIOR OF TENSIONED DOUBLY-CONNECTED PLATES

A THESIS

Presented to

The Faculty of the Division of Graduate

Studies and Research

by

Guerry Clark Backer

In Partial Fulfillment

of the Requirements for the Degree

Doctor of Philosophy

in the School of Aerospace Engineering

Georgia Institute of Technology

August 1972

STATIC AND DYNAMIC BEHAVIOR
OF TENSIONED DOUBLY - CONNECTED PLATES

Approved:

Chairman R. L. Carlson

C. V. Smith

G. A. Pierce

Date approved by Chairman: 8/21/72

In presenting the dissertation as a partial fulfillment of the requirements for an advanced degree from the Georgia Institute of Technology, I agree that the Library of the Institute shall make it available for inspection and circulation in accordance with its regulations governing materials of this type. I agree that permission to copy from, or to publish from, this dissertation may be granted by the professor under whose direction it was written, or, in his absence, by the Dean of the Graduate Division when such copying or publication is solely for scholarly purposes and does not involve potential financial gain. It is understood that any copying from, or publication of, this dissertation which involves potential financial gain will not be allowed without written permission.

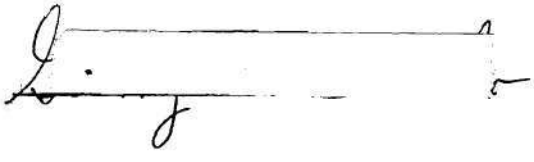

7/25/68

ACKNOWLEDGMENTS

I would like to express my sincere thanks to my dissertation advisor, Robert L. Carlson, for his ideas, direction and encouragement during the course of this research work. My many hours of consultation with him were invaluable in the completion of this work.

Grateful appreciation is extended to Dr. C. V. Smith for his constructive criticism and valuable suggestions for improvement. I would also like to thank the other members of my reading committee, Dr. G. A. Pierce, Dr. J. M. Anderson and Dr. D. J. McGill, for their contributions.

I would like to acknowledge the U. S. Army Research Office-Durham (Contract No. DAH-C04-68C 0004) for sponsoring this research project. Also I would like to thank Lockheed Aircraft Corporation for awarding me a fellowship.

I am grateful to John Madden for conducting the experimental investigations described in this manuscript.

Special thanks go to Mrs. Ruth Shaw for typing the rough draft and final manuscript. The neat appearance of this manuscript can be attributed to her skill.

An expression of thanks is given to my parents for their financial assistance and encouragement.

My deepest appreciation goes to my wife, Lynn. Her love, encouragement and understanding beyond all else are responsible for the completion of this work.

TABLE OF CONTENTS

LIST OF TABLES

LIST OF ILLUSTRATIONS

NOMENCLATURE

$[A]$	real square matrix
a	radius of circular inner boundary of plate
$a_{k\ell mn}$	coefficients associated with the mass of the system
$[B]$	real square matrix
b	radius of circular outer boundary of plate
$b_{k\ell mn}$	coefficients associated with the strain energy in the system
$[C]$	real square matrix
$c_{k\ell mn}$	coefficients associated with the static loading
D	plate bending stiffness, $Eh^3/12(1-\nu^2)$
$[D]$	real square matrix
ds	differential length
d	coefficients associated with the dynamic loading
E	Young's modulus
$E(m)$	value of the m^{th} exponential integral
e	height of elliptic hole
f_{mn}	unknown coefficients
$\{f\}$	column matrix of the coefficients f_{mn}
G_1	magnitude of $\vec{g}_1$
G_2	magnitude of $\vec{g}_2$
$\vec{g}_1$	vector tangent to curve α_2 equal a constant

$\vec{g}_2$	vector tangent to curve α_1 equal a constant
h	thickness of plate
[I]	identity matrix
$\vec{i}$	unit vector in x-direction
$\vec{j}$	unit vector in y-direction
K	extensional stiffness, $Eh/(1-\nu^2)$
K_F	frequency coefficient, $\omega a^2 \sqrt{\rho h/D}$
K_F^1	smallest eigenvalue
K_L	loading coefficient, $\gamma a^2/D$
K_L^1	lowest positive eigenvalue
k	integer
$\vec{k}$	unit vector in z-direction
ℓ	integer
M_{11}	bending moment distribution associated with σ_{11}
M_{22}	bending moment distribution associated with σ_{22}
M_{12}	twisting moment distribution associated with σ_{12}
M_{rr}	bending moment distribution associated with σ_{rr}
$M_{r\theta}$	twisting moment distribution associated with $\sigma_{r\theta}$
m	integer
N_{11}	stress resultant associated with σ_{11}
N_{11}^S	normalized static component of N_{11}

N_{11}^{D} normalized dynamic component of N_{11}

N_{22} stress resultant associated with σ_{22}

N_{22}^{S} normalized static component of N_{22}

N_{22}^{D} normalized dynamic component of N_{22}

N_{12} stress resultant associated with σ_{12}

N_{12}^{S} normalized static component of N_{12}

N_{12}^{D} normalized dynamic component of N_{12}

N_{rr} normal resultant in r-direction

N_{rr}^{S} normalized static component of N_{rr}

N_{rr}^{D} normalized dynamic component of N_{rr}

$N_{\theta\theta}$ normal stress resultant in θ-direction

$N_{\theta\theta}^{S}$ normalized static component of $N_{\theta\theta}$

$N_{\theta\theta}^{D}$ normalized dynamic component of $N_{\theta\theta}$

$N_{r\theta}$ shearing stress resultant

$N_{r\theta}^{S}$ normalized static component of $N_{r\theta}$

$N_{r\theta}^{D}$ normalized dynamic component of $N_{r\theta}$

$\bar{N}$ stress resultant on boundary of plate

$\bar{N}_{xx}$ uniform boundary loading on rectangular plate

$\bar{N}^{S}_{xx}$	normalized static component of $\bar{N}_{xx}$
$\bar{N}^{D}_{xx}$	normalized dynamic component of $\bar{N}_{xx}$
N_{cr}	critical stress resultant for local buckling
n	integer
P	time dependent magnitude of force
P_o	static loading parameter
P_1	dynamic loading parameter
$\{p\}_k$	k^{th} column matrix of unknown coefficients
Q_1	transverse shear resultant on a plane with normal in α_1-direction
Q_2	transverse shear resultant on a plane with normal in α_2-direction
Q_r	transverse shear resultant on a plane with normal in r-direction
$[Q]$	real symmetric matrix
$\{q\}$	column matrix of unknown coefficients
$\{q\}_k$	k^{th} column matrix of unknown coefficients
r	polar coordinate direction
$\vec{r}$	position vector to point in undeformed body
$\vec{r}^{*}$	position vector to point in deformed body
S_{mn}	coefficient for satisfying natural boundary conditions
T	period of periodic function $\Psi(t)$
T_{mn}	coefficient for satisfting natural boundary conditions

t	variable of time
U	strain energy
$\vec{U}$	displacement vector
u	displacement component in α_1 direction, function of α_1, α_2 and t
u_1	displacement component in α_1-direction, function of α_1, α_2, z and t
u_2	displacement component in α_2-direction, function of α_1, α_2, z and t
u_z	displacement component in z-direction, function of α_1, α_2, z and t
v	displacement component in α_2-direction, function of α_1, α_2 and t
W_e	work done by external forces and inertia forces on body
W_i	work done by internal forces in body
w	displacement component in z-direction, function of α_1, α_2 and t
w_o	transverse motion of plate before disturbance is applied
w_1	transverse disturbance applied to plate
x	coordinate of point in undeformed body
x^*	coordinate of point in deformed body
$\{x\}$	column matrix of unknown coefficients
y	coordinate of point in undeformed body
y^*	coordinate of point in deformed body
$\{y\}$	column matrix of unknown coefficients
z	coordinate of point in undeformed body

z^*	coordinate of point in deformed body
α_1	curvilinear coordinate direction
α_2	curvilinear coordinate direction
β	dynamic loading parameter
γ	static loading parameter
Δ	value of determinant
δ	variation
ϵ	measure of strain
ϵ_{11}	total normal strain in α_1-direction
ϵ_{11}^0	midsurface normal strain component in α_1-direction
ϵ_{11}^1	bending strain component in α_1-direction
ϵ_{22}	total normal strain in α_2-direction
ϵ_{22}^0	midsurface normal strain component in α_2-direction
ϵ_{22}^1	bending strain component in α_2-direction
ϵ_{zz}	total normal strain in z-direction
ϵ_{12}	total shearing strain
ϵ_{12}^0	midsurface shearing strain component
ϵ_{12}^1	twisting strain component
ϵ_{1z}	shearing strain
ϵ_{2z}	shearing strain

θ	polar coordinate direction
λ	excitation frequency
μ	parameter
ν	Poisson's ratio
ξ	outer to inner boundary ratio
ρ	density
σ_{11}	normal stress in α_1-direction
σ_{22}	normal stress in α_2-direction
σ_{zz}	normal stress in z-direction
σ_{12}	shearing stress
ϕ	stress function
ϕ_o	stress function before disturbance is applied
ϕ_1	stress function due to disturbance
χ_{mn}	approximation functions
Ψ	function of time
ω	frequency
ω_N	lowest natural frequency
∇^2	Laplacian operator

SUMMARY

The work described in this dissertation was concerned with the static and dynamic behavior of doubly-connected plates subject to in-plane loading. Accordingly, the governing equations for this class of problems were derived and they are presented. The governing equations for the special cases of static stability and free vibration are obtained from the general equations by setting certain quantities to zero.

The results of an investigation of the local static stability of an infinite plate containing a circular hole are presented. A Galerkin method for solving the governing differential equations is used and the results are compared with those obtained by a previous investigator. It was found that the local critical tensile load differed by approximately a factor of two.

The results of a study of the natural vibration of a large circular plate containing a circular hole are also given. Static stability information is obtained from the approximate solution to the vibration problem. For large values of the ratio of the outer boundary radius to the inner boundary radius, the static stability results obtained in the vibration problem are compared with the results obtained in the static stability investigation. The results are in good agreement with each other.

The results of an experimental investigation of the dynamic behavior of two rectangular sheet specimens containing different shaped

openings are presented. One of the specimens had a centrally located circular hole and the other had a centrally located elliptic hole. The first part of the experiment involved finding the natural frequency of vibration of the specimens for different values of applied tensile load. The natural frequency for the specimen with a circular hole increased with increasing load. The natural frequency versus applied load curve for the specimen with the elliptic hole had three distinct regions; a region of increasing frequency, a region of decreasing frequency and then another region of increasing frequency.

The second part of the experimental investigation was concerned with the vibration behavior of the specimens when the applied tensile load varied with time. The results indicate that for a small value of the amplitude of the varying load, the natural frequency of the specimens is related to the excitation frequency by the integer values of 1, 2, 3, etc. The frequency ratios of 1/2, 1, 3/2, 2, etc. which are usually observed in the dynamic stability investigations of other structural elements were not obtained for the two specimens tested.

CHAPTER I

INTRODUCTION

Static and Dynamic Stability

Leonhard Euler [1] initiated the development of the theory for stability of equilibrium configurations of elastic bodies in 1744 when he solved the problem of a slender column loaded by axial compression forces (Figure 1). The concept of stability received little attention during Euler's lifetime because at that time it appeared to be of no practical value. The primary construction materials were wood and stone, and due to the relatively low strength of these materials, bodies designed to meet strength requirements were so stout that they never failed from being unstable. Only when the introduction of high strength steel as a construction material during the latter half of the nineteenth century did the problem of stability become important.

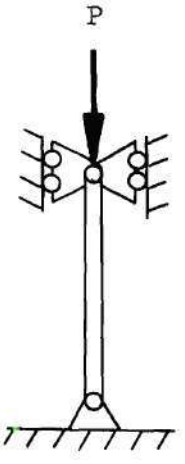

Figure 1. Euler Column

The theory of stability of equilibrium configurations of bodies under static loads (loads that are not a function of time) involves finding the positions of equilibrium of the body and then examining these positions to determine which are stable and which are unstable.

Problems of this type are called static stability problems due to the static nature of the loading. The stability information can be obtained mathematically by deriving the equations of motion of the body about an equilibrium position and examining the response of the body to a small, but otherwise, arbitrary disturbance applied to the body. The disturbance is specified by initial conditions as a small finite displacement of the body, a small finite velocity imparted to the body, or any combination of the two. For a linear analysis, an equilibrium position is said to be stable when all solutions to the equations of motion are bounded and unstable when any solution is unbounded.

It is possible, however, to consider stability problems of a more general nature in which the static stability information is obtained as a limiting case. These problems belong to the field of dynamic stability. Dynamic stability is the study of motion of a body or system of bodies which are excited by an external force system which possesses the following characteristic: At least one of the external forces must be time dependent and be applied in such a manner that an equivalent time independent load is able to induce loss of static stability.

To illustrate a problem of dynamic stability, consider the Euler-column (Figure 1). If the axial force is specified to have a magnitude that varies with time, the problem becomes one of studying longitudinal motion of the column. The equivalent time independent loading (in this example the equivalent time independent loading is one in which the direction and point of application of the axial force remain unchanged but the magnitude is not a function of time) reduces the dynamic stability problem to a static stability problem. An axial

load of the form $P_0 + P_1 \cos \lambda t$, where P_0 and P_1 are time independent amplitudes, λ is the frequency of excitation and t is the variable time, is a possible choice for the time dependent load. If the column is perfectly straight, it experiences only periodic longitudinal motion for any values of the force parameters, P_0, P_1 and λ. However, a small disturbance in the transverse direction can produce one of the following responses:

(1) the column experiences motion in the transverse direction which is bounded

or (2) the column experiences motion in the transverse direction which is unbounded.

For any arbitrary disturbance, the motion of the column is said to be stable in the first case and unstable in the second case. Whether the motion is stable or unstable is found to depend on the values of P_0, P_1 and λ. A stability plot can be made in parameter space (P_0, P_1 and λ space) by studying the motion of the column for particular combinations of the loading parameters.

Historical Background of Dynamic Stability

The first mathematical analysis of a problem in dynamic stability was performed by N. M. Beliaev [2] in 1924. Beliaev obtained the principal region of instability for the hinged column loaded by the force, $P(t) = P_0 + P_1 \cos \lambda t$. When he held the value of P_0 constant, he was able to plot the instability region in the $P_1 - \lambda$ plane.

The first person to treat the problem of thin elastic plates loaded by periodic in-plane loads was R. Einaudi [3] in 1936. Other

pioneers in the investigation of dynamic stability of plates were V. N. Chelomei [4] and V. A. Bodner [5]. Chelomei made use of an energy method to solve the problem of a hinged plate that was not perfectly flat. Bodner, independent of Chelomei, solved a series of problems of the dynamic stability of plates. For the hinged flat plate he obtained the exact solution, while for other edge conditions he obtained only approximate solutions.

One of the more recent investigators on the subject of dynamic stability of plates is V. V. Bolotin. He has developed solutions to both linear and non-linear dynamic stability of plate problems. These appear in his book [6], The Dynamic Stability of Elastic Systems, which was published in Russian in 1956, and translated to English in 1964.

J. H. Somerset and R. M. Evan-Iwanowski [7] in 1965 showed that in-plane inertia influences the frequencies associated with the instability zones of a rectangular plate with a concentrated edge mass only if the excitation frequency is close to one of the natural frequencies of in-plane vibration. Theoretical results of the problem were compared with experimental work [8] and were found to be in good agreement. In 1969 N. Willems and R. C. Duffield [9] solved the problem of the dynamic stability of a rectangular plate with closely spaced stiffners. They showed that the presence of stiffeners on the rectangular plate causes the instability regions to be larger than the corresponding regions for an unstiffened plate.

A description of the Russian accomplishments in the field of dynamic stability through the year 1951 is given by E. A. Beilin and G. Y. Dzhanelidze [10]. A complete summary of the work that has been

done on the dynamic stability of columns, arches, rings, plates and shells through the year 1965 is presented by R. M. Evan-Iwanowski [11].

Objective

Under certain conditions, doubly-connected plates loaded by in-plane time independent tensile forces on the outer boundary can undergo out-of-plane deflections in a local region on the inner boundary. This behavior is possible because of compressive stresses that are present in a local region at the inner boundary of the plate. When an equivalent time dependent loading (a loading with the same direction and point of application but a magnitude which is a function of time) acts on the outer boundary of such plates, the possibility of the plate being dynamically unstable in a local region of the plate exists.

The primary objective of the investigation described in this dissertation was to study the static and dynamic stability of structural elements of the type discussed above. Accordingly, the governing equations for this class of problems have been derived and they are presented. Since the dynamic behavior under constant load exhibits properties of the structural system which are of fundamental importance in the dynamic stability problem, it was also considered.

CHAPTER II

GOVERNING EQUATIONS

Introduction

The possibility of obtaining a simple solution of a given boundary-value problem often depends upon the choice of the coordinate system. This is particularly true when constant values of one or more of the coordinates define the region of the boundary in the problem under consideration. For example, cylindrical coordinates would be a good choice if a plate's boundary is formed by a circle, and elliptic-hyperbolic coordinates might be used for a plate with a boundary formed by an ellipse.

With the idea in mind of having available the governing equations in the coordinate system which affords the best possibility of obtaining a solution to a problem, the governing equations for dynamic stability of the plates are derived in curvilinear coordinates. This can be accomplished by letting the position of a point in a Cartesian coordinate system at time t be given by the vector,

$$\vec{r}(\alpha_1,\alpha_2,z,t) = x(\alpha_1,\alpha_2,t)\vec{i} + y(\alpha_1,\alpha_2,t)\vec{j} + z(t)\vec{k} \quad ,$$

where α_1 and α_2 are parameters that determine the values of x and y. The symbols $\vec{i}$, $\vec{j}$ and $\vec{k}$ denote unit vectors in the x, y, and z directions respectively (Figure 2). By fixing, in turn,

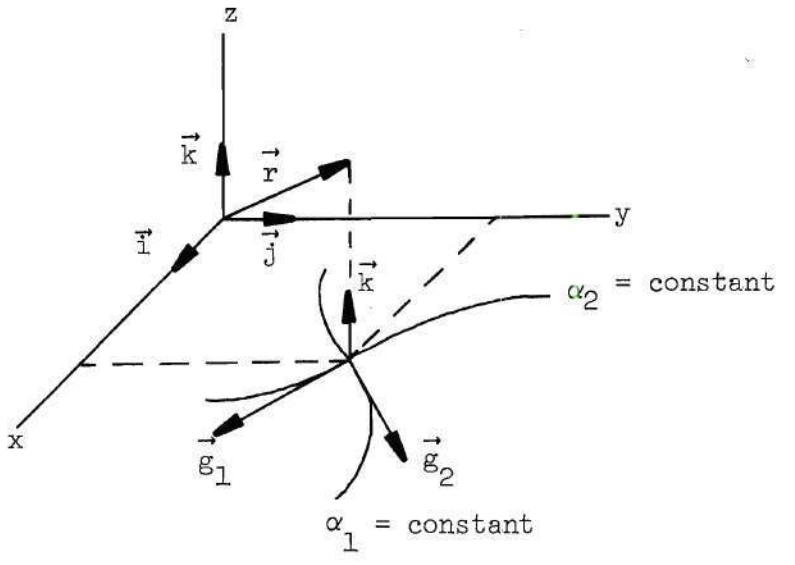

Figure 2. Coordinate System

one of the parameters and varying the other, a family of curves in the x - y plane is obtained. Vectors tangent to the curves of α_2 equal a constant and α_1 equal a constant are

$$\vec{g}_1 = \frac{\partial \vec{r}}{\partial \alpha_1} \quad \text{and} \quad \vec{g}_2 = \frac{\partial \vec{r}}{\partial \alpha_2}$$

respectively. The magnitudes of these vectors can be obtained by taking the dot product of each vector with itself. These magnitudes are denoted by the symbols G_1 and G_2 and are defined as

$$\left.\begin{aligned} G_1 &= \left[\vec{g}_1 \cdot \vec{g}_1\right]^{\frac{1}{2}} = \left[\left(\frac{\partial x}{\partial \alpha_1}\right)^2 + \left(\frac{\partial y}{\partial \alpha_1}\right)^2\right]^{\frac{1}{2}} \\ \text{and} \\ G_2 &= \left[\vec{g}_2 \cdot \vec{g}_2\right]^{\frac{1}{2}} = \left[\left(\frac{\partial x}{\partial \alpha_2}\right)^2 + \left(\frac{\partial y}{\partial \alpha_2}\right)^2\right]^{\frac{1}{2}} . \end{aligned}\right\} \quad (1)$$

If the family of curves in the x - y plane forms an orthogonal system (that is, curves of α_1 equal a constant intersect curves α_2 equal a constant at right angles), the dot product of the vector $\vec{g}_1$ with $\vec{g}_2$ is equal to zero. The final governing equations then contain terms involving only G_1 and G_2 in addition to the physical quantities of displacement, stress, etc. Thus, knowing the transformation equations from Cartesian coordinates to the coordinate system deemed appropriate for a particular problem, the values of G_1 and G_2 can be calculated. The field equations can then be obtained by introducing the calculated values of G_1 and G_2.

Strain-Displacement Equations

Consider a body whose undeformed position at time $t = 0$ is given by the coordinates x, y, and z (Figure 3). The position vector of a point located in the undeformed body is

$$\vec{r}(\alpha_1,\alpha_2,z,0) = x(\alpha_1,\alpha_2,0)\vec{i} + y(\alpha_1,\alpha_2,0)\vec{j} + z(0)\vec{k} \quad .$$

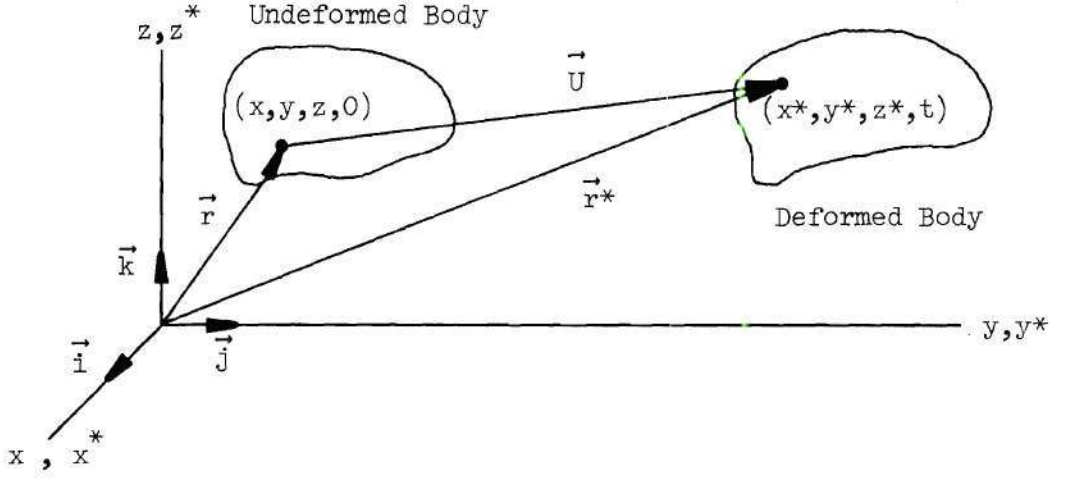

Figure 3. Deformation of Body

At some later time t the point x, y and z is located at some other point x^*, y^* and z^*. If a Lagrangian description of deformation is used, the position vector of the point in the deformed body is

$$\vec{r}^*(\alpha_1,\alpha_2,z,t) = x^*(\alpha_1,\alpha_2,z,t)\vec{i} + y^*(\alpha_1,\alpha_2,z,t)\vec{j} + z^*(\alpha_1,\alpha_2,z,t)\vec{k} \ .$$

It proves convenient to adopt a measure of strain at a point which is defined in terms of the differentials of the vectors $\vec{r}$ and $\vec{r}^*$ as

$$\epsilon = 1/2(d\vec{r}^* \cdot d\vec{r}^* - d\vec{r} \cdot d\vec{r})/(d\vec{r} \cdot d\vec{r}) \ .$$

The definition of strain can be expressed as

$$\epsilon = (d\vec{r} \cdot d\vec{U} + 1/2\ d\vec{U} \cdot d\vec{U})/(d\vec{r} \cdot d\vec{r}) \qquad (2)$$

by introducing the displacement vector (Figure 3)

$$\vec{U} = \vec{r}^* - \vec{r} \ .$$

Writing the displacement vector in component form as

$$\vec{U} = \frac{u_1}{G_1}\vec{g}_1 + \frac{u_2}{G_2}\vec{g}_2 + u_z\vec{k} \ ,$$

carrying out the indicated vector algebra in Equation (2), using the identities given in Appendix A, and neglecting all non-linear terms except

$$\left(\frac{\partial u_z}{\partial \alpha_1}\right)^2, \quad \left(\frac{\partial u_z}{\partial \alpha_2}\right)^2 \quad \text{and} \quad \left(\frac{\partial u_z}{\partial \alpha_1}\right)\left(\frac{\partial u_z}{\partial \alpha_2}\right),$$

gives the strain-displacement equations. They are

$$\epsilon = \epsilon_{11}(G_1 d\alpha_1/ds)^2 + \epsilon_{22}(G_2 d\alpha_2/ds)^2$$

$$+ \epsilon_{zz}(dz/ds)^2 + 2\epsilon_{12}(G_1 d\alpha_1/ds)(G_2 d\alpha_2/ds)$$

$$+ 2\epsilon_{1z}(G_1 d\alpha_1/ds)(dz/ds) + 2\epsilon_{2z}(G_2 d\alpha_2/ds)(dz/ds),$$

where

$$\epsilon_{11} = \frac{\partial}{\partial \alpha_1}\left(\frac{u_1}{G_1}\right) + \frac{1}{2G_1^2}\left[\frac{u_1}{G_1}\frac{\partial G_1^2}{\partial \alpha_1} + \frac{u_2}{G_2}\frac{\partial G_1^2}{\partial \alpha_2} + \left(\frac{\partial u_z}{\partial \alpha_1}\right)^2\right] \tag{3}$$

$$\epsilon_{22} = \frac{\partial}{\partial \alpha_2}\left(\frac{u_2}{G_2}\right) + \frac{1}{2G_2^2}\left[\frac{u_1}{G_1}\frac{\partial G_2^2}{\partial \alpha_1} + \frac{u_2}{G_2}\frac{\partial G_2^2}{\partial \alpha_2} + \left(\frac{\partial u_z}{\partial \alpha_2}\right)^2\right] \tag{4}$$

$$\epsilon_{zz} = \frac{\partial u_z}{\partial z} \tag{5}$$

$$2\epsilon_{12} = \frac{1}{G_1 G_2}\left[G_2^2 \frac{\partial}{\partial \alpha_1}\left(\frac{u_2}{G_2}\right) + G_1^2 \frac{\partial}{\partial \alpha_2}\left(\frac{u_1}{G_1}\right) + \frac{\partial u_z}{\partial \alpha_1}\frac{\partial u_z}{\partial \alpha_2}\right] \tag{6}$$

$$2\epsilon_{1z} = \frac{1}{G_1}\left[\frac{\partial u_z}{\partial \alpha_1} + G_1 \frac{\partial}{\partial z}\left(u_1\right)\right] \tag{7}$$

$$2\epsilon_{2z} = \frac{1}{G_2}\left[\frac{\partial u_z}{\partial \alpha_2} + G_2 \frac{\partial}{\partial z}\left(u_2\right)\right] \tag{8}$$

and ds is the magnitude of $\vec{dr}$. The strain component ϵ_{11} is a measure of the change in length of the line segment $G_1 d\alpha_1$. The strain component ϵ_{12} is the change in angle between the line segments $G_1 d\alpha_1$ and $G_2 d\alpha_2$. A similar physical interpretation can be given to the two other extensional strain components ϵ_{22} and ϵ_{zz}, and the two other shearing strain components ϵ_{1z} and ϵ_{2z}.

Retaining some non-linear terms in the derivation of the governing equations was first introduced by T. von Karman in 1910 in order to treat thin plates which experience moderately large deflections. Karman suggested that the rotations about the in-plane axes be retained since they are large compared to the other rotations for moderately large deflections of plates.

The displacement component u_z in the above equations is a function of α_1, α_2, z and t. If it is assumed that normals to the reference surface are inextensible ($\epsilon_{zz} = 0$; one of the Kirchhoff-Love hypotheses), the displacement component u_z becomes a function of only α_1, α_2 and t. This can be shown by considering Equation (5) which becomes

$$\frac{\partial u_z}{\partial z} = 0 \tag{9}$$

upon adopting this assumption. Integration of Equation (9) with respect to

z yields a function of α_1, α_2 and t which may be written as

$$u_z = w(\alpha_1,\alpha_2,t) \ . \tag{10}$$

With this result and the assumption that normals to the reference surface before deformation remain normal to the reference surface after deformation ($\varepsilon_{1z} = 0$ and $\varepsilon_{2z} = 0$; second of the Kirchhoff-Love hypotheses), the z dependence in the displacement components $u_1(\alpha_1,\alpha_2,z,t)$ and $u_2(\alpha_1,\alpha_2,z,t)$ can be determined. The assumption that $\varepsilon_{1z} = 0$ implies that Equation (7) is equal to zero, so

$$\frac{\partial u_z}{\partial \alpha_1} + G_1 \frac{\partial}{\partial z}\left(u_1\right) = 0 \ .$$

Integrating this equation with respect to z and using the result that u_z is not a function of z from Equation (10) produces the expression

$$u_1(\alpha_1,\alpha_2,z,t) = u(\alpha_1,\alpha_2,t) - \frac{z}{G_1} \frac{\partial}{\partial \alpha_1} w(\alpha_1,\alpha_2,t) \ . \tag{11}$$

In a similar manner, the expression

$$u_2(\alpha_1,\alpha_2,z,t) = v(\alpha_1,\alpha_2,t) - \frac{z}{G_2} \frac{\partial}{\partial \alpha_2} w(\alpha_1,\alpha_2,t) \tag{12}$$

can be obtained by equating Equation (8) to zero ($\varepsilon_{2z} = 0$) and then integrating with respect to z.

The desired strain-displacement equations are given by substitut-

ing the expressions for u_1, u_2 and u_z of Equations (10, 11 and 12) respectively, into Equations(3, 4 and 6). These equations are

$$\left.\begin{aligned} \epsilon_{11} &= \epsilon^0_{11} + z\epsilon^1_{11} \\ \epsilon_{22} &= \epsilon^0_{22} + z\epsilon^1_{22} \\ \epsilon_{12} &= \epsilon^0_{12} + z\epsilon^1_{12} \quad , \end{aligned}\right\} \tag{13}$$

where

$$\left.\begin{aligned} \epsilon^0_{11} &= \frac{1}{G_1}\frac{\partial u}{\partial \alpha_1} + \frac{v}{G_1 G_2}\frac{\partial G_1}{\partial \alpha_2} + \frac{1}{2G_1^2}\left(\frac{\partial w}{\partial \alpha_1}\right)^2 \\ \epsilon^0_{22} &= \frac{1}{G_2}\frac{\partial v}{\partial \alpha_2} + \frac{u}{G_1 G_2}\frac{\partial G_2}{\partial \alpha_1} + \frac{1}{2G_2^2}\left(\frac{\partial w}{\partial \alpha_2}\right)^2 \\ 2\epsilon^0_{12} &= \frac{1}{G_1}\frac{\partial v}{\partial \alpha_1} - \frac{v}{G_1 G_2}\frac{\partial G_2}{\partial \alpha_1} + \frac{1}{G_2}\frac{\partial u}{\partial \alpha_2} \\ &\quad - \frac{u}{G_1 G_2}\frac{\partial G_1}{\partial \alpha_2} + \frac{1}{G_1 G_2}\frac{\partial w}{\partial \alpha_1}\frac{\partial w}{\partial \alpha_2} \end{aligned}\right\} \tag{14}$$

$$
\left.
\begin{aligned}
-\epsilon^1_{11} &= \frac{1}{G_1}\frac{\partial}{\partial\alpha_1}\left(\frac{1}{G_1}\frac{\partial w}{\partial\alpha_1}\right) + \frac{1}{G_2^2 G_1}\frac{\partial G_1}{\partial\alpha_2}\frac{\partial w}{\partial\alpha_2} \\
-\epsilon^1_{22} &= \frac{1}{G_2}\frac{\partial}{\partial\alpha_2}\left(\frac{1}{G_2}\frac{\partial w}{\partial\alpha_2}\right) + \frac{1}{G_1^2 G_2}\frac{\partial G_2}{\partial\alpha_1}\frac{\partial w}{\partial\alpha_1} \\
-2\epsilon^1_{12} &= \frac{1}{G_1}\frac{\partial}{\partial\alpha_1}\left(\frac{1}{G_2}\frac{\partial w}{\partial\alpha_2}\right) - \frac{1}{G_2^2 G_1}\frac{\partial G_2}{\partial\alpha_1}\frac{\partial w}{\partial\alpha_2} \\
&\quad + \frac{1}{G_2}\frac{\partial}{\partial\alpha_2}\left(\frac{1}{G_1}\frac{\partial w}{\partial\alpha_1}\right) - \frac{1}{G_1^2 G_2}\frac{\partial G_1}{\partial\alpha_2}\frac{\partial w}{\partial\alpha_1} .
\end{aligned}
\right\} \quad (15)
$$

Stress-Strain Equations

The stress-strain equations for a thin plate made of a material which is isotropic and linear elastic are

$$
\left.
\begin{aligned}
\epsilon_{11} &= \frac{1}{E}\left(\sigma_{11} - \nu\sigma_{22}\right) \\
\epsilon_{22} &= \frac{1}{E}\left(\sigma_{22} - \nu\sigma_{11}\right) \\
\text{and} \qquad \epsilon_{12} &= \frac{1+\nu}{E}\sigma_{12} .
\end{aligned}
\right\} \quad (16)
$$

Since the plate is assumed to be thin, the normal stress σ_{zz} can be neglected. The strains ϵ_{1z}, ϵ_{2z}, and ϵ_{zz} are equal to zero from the Kirchhoff-Love hypothesis used in obtaining the strain-displacement equations in the previous section. Solving Equations (16) for the

stresses in terms of the strains produces the equations

$$\left.\begin{aligned} \sigma_{11} &= \frac{E}{1-\nu^2}\left(\epsilon_{11} + \nu\,\epsilon_{22}\right) \\ \sigma_{22} &= \frac{E}{1-\nu^2}\left(\epsilon_{22} + \nu\,\epsilon_{11}\right) \\ \text{and} \qquad \sigma_{12} &= \frac{E}{1+\nu}\left(\epsilon_{12}\right) \quad . \end{aligned}\right\} \tag{17}$$

The substitution of these equations into the stress resultant and moment definitions*

$$\left.\begin{aligned} N_{11} &= \int_z \sigma_{11}\, dz & N_{22} &= \int_z \sigma_{22}\, dz \\ N_{12} &= \int_z \sigma_{12}\, dz & M_{11} &= \int_z z\,\sigma_{11}\, dz \\ M_{22} &= \int_z z\,\sigma_{22}\, dz \quad \text{and} & M_{12} &= \int_z z\,\sigma_{12}\, dz \quad , \end{aligned}\right\} \tag{18}$$

results in the following six equations:

* The subscript on the integral sign indicates the integration is not indefinite but extends across the thickness of the plate.

$$
\left.
\begin{aligned}
N_{11} &= \frac{E}{1-\nu^2} \int_z (\epsilon_{11} + \nu\, \epsilon_{22})\, dz \\
N_{22} &= \frac{E}{1-\nu^2} \int_z (\epsilon_{22} + \nu\, \epsilon_{11})\, dz \\
N_{12} &= \frac{E}{1+\nu} \int_z \epsilon_{12}\, dz \\
M_{11} &= \frac{E}{1-\nu^2} \int_z z(\epsilon_{11} + \nu\, \epsilon_{22})\, dz \\
M_{22} &= \frac{E}{1-\nu^2} \int_z z(\epsilon_{22} + \nu\, \epsilon_{11})\, dz \\
\text{and} \qquad M_{12} &= \frac{E}{1+\nu} \int_z z\, \epsilon_{12}\, dz \quad .
\end{aligned}
\right\} \qquad (19)
$$

The sign convention for the stress resultants and moments is given in Figure 4.

From the previous section on strain-displacement equations, the dependence of the strains ϵ_{11}, ϵ_{22} and ϵ_{12} on the variable z is given in Equations (13),

$$\epsilon_{11} = \epsilon^0_{11} + z\, \epsilon^1_{11}$$

$$\epsilon_{22} = \epsilon^0_{22} + z\, \epsilon^1_{22}$$

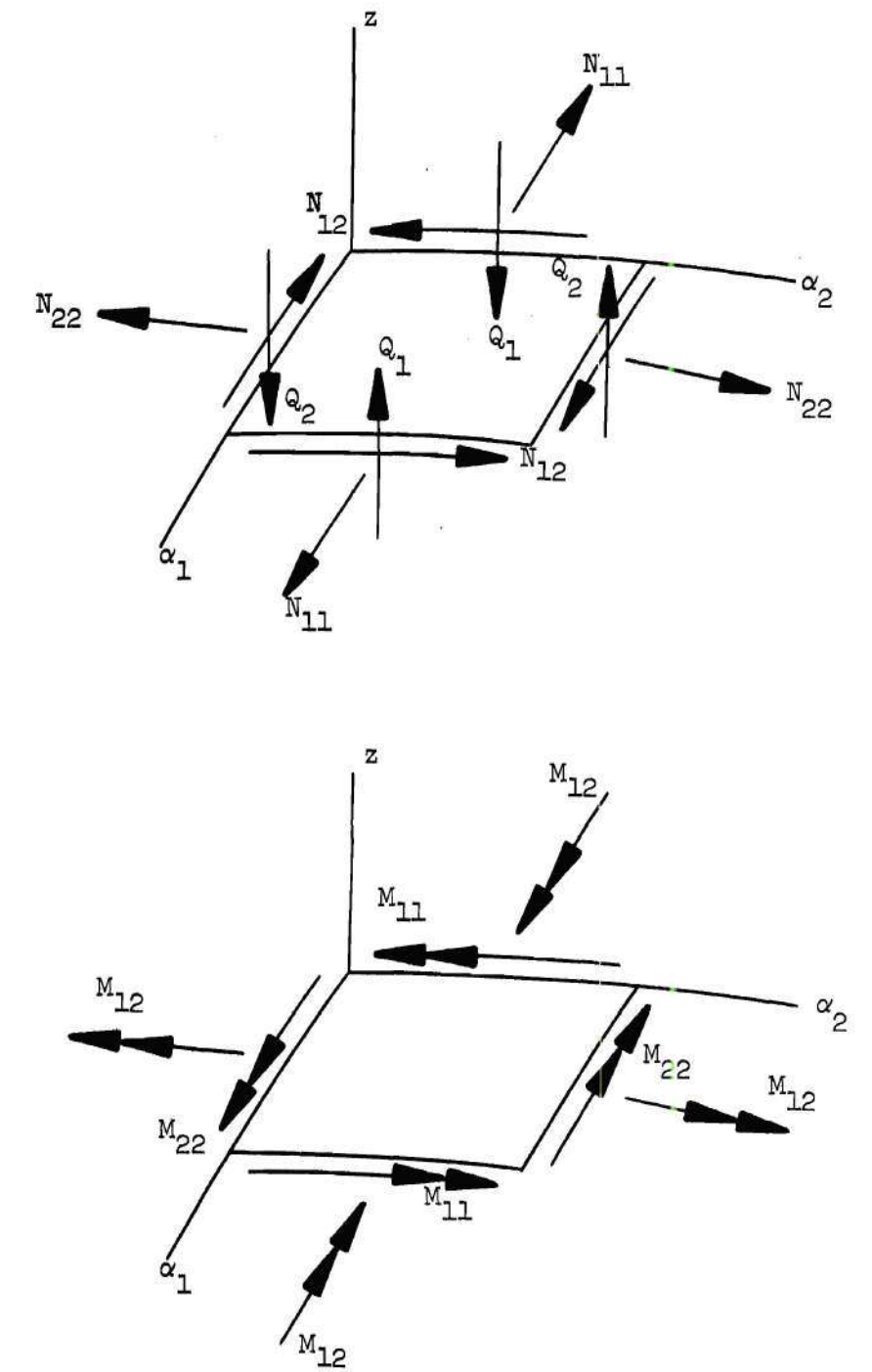

Right-hand Rule

Figure 4. Sign Convention

and $$\epsilon_{12} = \epsilon^0_{12} + z\,\epsilon^1_{12} \quad .$$

The terms ϵ^0_{11}, ϵ^0_{22}, ϵ^0_{12}, ϵ^1_{11}, ϵ^1_{22} and ϵ^1_{12} are functions of only the coordinate variables α_1 and α_2, and the time variable t. If the reference surface is chosen to be the mid-plane of the plate, the desired form of the stress-strain equations is obtained by substituting the above equations into Equations (19) and performing the integrations with respect to z. These equations are

$$\left.\begin{aligned} N_{11} &= K(\epsilon^0_{11} + \nu\,\epsilon^0_{22}) \\ N_{22} &= K(\epsilon^0_{22} + \nu\,\epsilon^0_{11}) \\ N_{12} &= (1 - \nu)K\,\epsilon^0_{12} \end{aligned}\right\} \quad (20)$$

$$\left.\begin{aligned} M_{11} &= D(\epsilon^1_{11} + \nu\,\epsilon^1_{22}) \\ M_{22} &= D(\epsilon^1_{22} + \nu\,\epsilon^1_{11}) \\ M_{12} &= (1 - \nu)\,D\,\epsilon^1_{12} \quad . \end{aligned}\right\} \quad (21)$$

and

The symbols K and D are the plate extensional stiffness

$$K = \frac{Eh}{(1-\nu^2)} \quad ,$$

and the plate bending stiffness,

$$D = \frac{Eh^3}{12(1-\nu^2)} \quad .$$

Equations of Motion

At a given time t, a body in motion can be considered to be in a state of equilibrium if the inerta forces are taken into account (d'Alembert's Principle). Using this principle to put the body in a state of equilibrium, the principle of virtual work can then be used to obtain the equations of motion. The principle of virtual work states:

> A body is in equilibrium if and only if for any virtual displacement the work done by the internal forces in the body plus the work done by the external forces on the body is equal to zero.

A virtual displacement is defined as a compatible displacement in which the forces, both internal and external, remain constant during the displacement. In mathematical form the principle of virtual work is

$$\delta W_i + \delta W_e = 0 \quad ,$$

where δW_i is the work done by the internal forces during the virtual displacement, and δW_e is the work done by the external forces and

inertia forces during the virtual displacement. If a strain energy functional exists such that δW_i can be written as

$$\delta W_i = - \delta U,$$

the mathematical expression for the principle of virtual work becomes

$$\delta U = \delta W_e \ . \tag{22}$$

Since the stress-strain equations are linear, the strain energy functional for two dimensional plate theory can be expressed as

$$U = \frac{1}{2} \int_{\alpha_1} \int_{\alpha_2} \int_z \left(\sigma_{11} \epsilon_{11} + \sigma_{22} \epsilon_{22} + 2 \sigma_{12} \epsilon_{12} \right) G_1 G_2 \, dz \, d\alpha_2 \, d\alpha_1 \ .$$

Substituting the value of the strains given in Equations (13) and using the stress resultant and moment definitions, Equations (18), the strain energy becomes

$$U = \frac{1}{2} \int_{\alpha_1} \int_{\alpha_2} \left(N_{11} \epsilon^0_{11} + N_{22} \epsilon^0_{22} + 2N_{12} \epsilon^0_{12} \right) G_1 G_2 \, d\alpha_2 \, d\alpha_1 \tag{23}$$

$$+ \frac{1}{2} \int_{\alpha_1} \int_{\alpha_2} \left(M_{11} \epsilon^1_{11} + M_{22} \epsilon^1_{22} + 2M_{12} \epsilon^1_{12} \right) G_1 G_2 \, d\alpha_2 \, d\alpha_1 \ .$$

This expression for U can be expressed in terms of the displacements u, v and w by use of Equations (14) and (15). After making the

substitution, the change in strain energy due to the virtual displacements δu, δv and δw can be calculated.

The work done by the external forces and inertia forces during the virtual displacements δu, δv and δw is given by the expression

$$\delta W_e = - \int_{\alpha_1} \int_{\alpha_2} \rho h \left(\frac{\partial^2 u}{\partial t^2} \delta u + \frac{\partial^2 v}{\partial t^2} \delta v + \frac{\partial^2 w}{\partial t^2} \delta w \right) G_1 G_2 \, d\alpha_2 \, d\alpha_1 \qquad (24)$$

$$+ \int_{\alpha_2} \left(\bar{N}_{11} \delta u + \bar{N}_{12} \delta v \right) G_2 \Big|_{\alpha_1} d\alpha_2$$

if it is assumed that

(1) the boundaries of the plate are specified by curves of α_1 equal a constant and

(2) the only external forces acting on the plate are the in-plane forces $\bar{N}_{11}$ and $\bar{N}_{12}$.

The bar on the stress resultants indicate that they are acting on the boundaries of the plate.

The principle of virtual work can now be used to obtain the equations of motion for the plate by

(1) calculating the change in U, δu, from Equation (23) due to the virtual displacements δu, δv and δw

(2) integrating several of the terms in the resulting expression for δU by parts and

(3) substituting this value of δU and the value of δW_e into Equation (22) which is the mathematical expression for the principle of virtual work.

After performing the above operation, the resulting expression is

$$- \int_{\alpha_1}\int_{\alpha_2} \Big\{ \Big[\frac{\partial}{\partial\alpha_1}\left(G_2 N_{11}\right) - \frac{\partial G_2}{\partial\alpha_1} N_{22} + \frac{1}{G_1}\frac{\partial}{\partial\alpha_2}\left(G_1^2 N_{12}\right) - \rho h\, G_1 G_2 \frac{\partial^2 u}{\partial t^2}\Big]\delta u \qquad (25)$$

$$+ \Big[\frac{\partial}{\partial\alpha_2}\left(G_1 N_{22}\right) - \frac{\partial G_1}{\partial\alpha_2} N_{11} + \frac{1}{G_2}\frac{\partial}{\partial\alpha_1}\left(G_2^2 N_{12}\right) - \rho h\, G_1 G_2 \frac{\partial^2 v}{\partial t^2}\Big]\delta v$$

$$+ \Big[\frac{\partial}{\partial\alpha_1}\left(G_2 Q_1\right) + \frac{\partial}{\partial\alpha_2}\left(G_1 Q_2\right) + \frac{\partial}{\partial\alpha_1}\left(\frac{G_2}{G_1} N_{11}\frac{\partial w}{\partial\alpha_1}\right)$$

$$+ \frac{\partial}{\partial\alpha_2}\left(\frac{G_1}{G_2} N_{22}\frac{\partial w}{\partial\alpha_2}\right) + \frac{\partial}{\partial\alpha_1}\left(N_{12}\frac{\partial w}{\partial\alpha_2}\right) + \frac{\partial}{\partial\alpha_2}\left(N_{12}\frac{\partial w}{\partial\alpha_1}\right)$$

$$- \rho h\, G_1 G_2 \frac{\partial^2 w}{\partial t^2}\Big]\delta w\Big\}\, d\alpha_2\, d\alpha_1 + \int_{\alpha_2}\Big\{\Big[N_{11} - \bar{N}_{11}\Big]\delta u$$

$$+ \Big[N_{12} - \bar{N}_{12}\Big]\delta v + \Big[Q_1 + \frac{1}{G_2}\frac{\partial M_{12}}{\partial\alpha_2} + N_{11}\frac{1}{G_1}\frac{\partial w}{\partial\alpha_1}$$

$$+ N_{12}\frac{1}{G_2}\frac{\partial w}{\partial\alpha_2}\Big]\delta w - \Big[\frac{1}{G_1} M_{11}\Big]\frac{\partial\delta w}{\partial\alpha_1}\Big\}\, G_2 \Big|_{\alpha_1}\, d\alpha_2 = 0 \quad ,$$

where Q_1 and Q_2 are defined as

$$\left.\begin{aligned} Q_1 &= \frac{1}{G_1 G_2}\left[\frac{\partial}{\partial\alpha_1}\left(G_2 M_{11}\right) - \frac{\partial G_2}{\partial\alpha_1} M_{22} + \frac{\partial}{\partial\alpha_2}\left(G_1 M_{12}\right) + \frac{\partial G_1}{\partial\alpha_2} M_{12}\right] \\ Q_2 &= \frac{1}{G_1 G_2}\left[\frac{\partial}{\partial\alpha_2}\left(G_1 M_{22}\right) - \frac{\partial G_1}{\partial\alpha_2} M_{11} + \frac{\partial}{\partial\alpha_1}\left(G_2 M_{12}\right) + \frac{\partial G_2}{\partial\alpha_1} M_{12}\right] \end{aligned}\right\} \quad (26)$$

It can be shown [12] that the quantities Q_1 and Q_2 are transverse shear resultants. The sign convention for Q_1 and Q_2 is shown in Figure 4.

Since δu, δv and δw are independent virtual displacements, one possible set of values is

$$\delta u \neq 0, \quad \delta v = 0 \quad \text{and} \quad \delta w = 0 .$$

Substituting these values into Equation (25) and appealing to the fundamental theorem of the calculus of variations yields

$$\frac{\partial}{\partial\alpha_1}\left(G_2 N_{11}\right) - \frac{\partial G_2}{\partial\alpha_1} N_{22} + \frac{1}{G_1}\frac{\partial}{\partial\alpha_2}\left(G_1^2 N_{12}\right) = \rho h\, G_1 G_2 \frac{\partial^2 u}{\partial t^2} , \quad (27)$$

and either $N_{11} = \bar{N}_{11}$ or $u = 0$.

Another possible set of values for δu, δv and δw is

$$\delta u = 0, \quad \delta v \neq 0 \quad \text{and} \quad \delta w = 0 .$$

The substitution of these values into Equation (25) and the application of the fundamental theorem of the calculus of variations produces the following condition:

$$\frac{\partial}{\partial \alpha_2}\left(G_1 N_{22}\right) - \frac{\partial G_1}{\partial \alpha_2} N_{11} + \frac{1}{G_2}\frac{\partial}{\partial \alpha_1}\left(G_2^2 N_{12}\right) = \rho h G_1 G_2 \frac{\partial^2 v}{\partial t^2} , \tag{28}$$

and either $N_{12} = \bar{N}_{12}$ or $v = 0$.

If the values of δu equal to zero and δv equal to zero are substituted into Equation (25) leaving the value of δw unspecified and Equations (27) and (28) are used to simplify the in-plane stress resultant terms, the equation

$$\int_{\alpha_1} \int_{\alpha_2} \left\{ \frac{1}{G_1 G_2} \left[\frac{\partial}{\partial \alpha_1} \left(G_2 Q_1 \right) + \frac{\partial}{\partial \alpha_2} \left(G_1 Q_2 \right) \right] + N_{11} \left[\frac{1}{G_1} \frac{\partial}{\partial \alpha_1} \left(\frac{1}{G_1} \frac{\partial w}{\partial \alpha_1} \right) \right. \right. \tag{29}$$

$$+ \frac{1}{G_1 G_2} \frac{\partial G_1}{\partial \alpha_2} \frac{\partial w}{\partial \alpha_2} \Big] + N_{22} \left[\frac{1}{G_2} \frac{\partial}{\partial \alpha_2} \left(\frac{1}{G_2} \frac{\partial w}{\partial \alpha_2} \right) \right.$$

$$\left. + \frac{1}{G_1^2 G_2} \frac{\partial G_2}{\partial \alpha_1} \frac{\partial w}{\partial \alpha_1} \right] + 2N_{12} \left[\frac{1}{G_2} \frac{\partial}{\partial \alpha_2} \left(\frac{1}{G_1} \frac{\partial w}{\partial \alpha_1} \right) \right.$$

$$\left. - \frac{1}{G_1 G_2^2} \frac{\partial G_2}{\partial \alpha_1} \frac{\partial w}{\partial \alpha_2} \right] + \rho h \left[\frac{1}{G_1} \frac{\partial^2 u}{\partial t^2} \frac{\partial w}{\partial \alpha_1} + \frac{1}{G_2} \frac{\partial^2 v}{\partial t^2} \frac{\partial w}{\partial \alpha_2} - \frac{\partial^2 w}{\partial t^2} \right] \Big\} \delta w \, G_1 G_2 d\alpha_2 d\alpha_1$$

$$+ \int_{\alpha_2} \left\{ Q_1 + \frac{1}{G_2} \frac{\partial M_{12}}{\partial \alpha_2} + N_{11} \frac{1}{G_1} \frac{\partial w}{\partial \alpha_1} + N_{12} \frac{1}{G_2} \frac{\partial w}{\partial \alpha_2} \right\} \delta w \, G_2 \Big|_{\alpha_1} d\alpha_2$$

$$- \int_{\alpha_2} \left\{ \frac{1}{G_1} M_{11} \right\} \frac{\partial \delta w}{\partial \alpha_1} \, G_2 \Big|_{\alpha_1} d\alpha_2 = 0$$

is obtained. The shear resultants Q_1 and Q_2 in the first integral of Equation (29) can be expressed in terms of the deflection component w by using Equations (26), (21) and (15). Equation (29) then becomes

$$\int_{\alpha_1}\int_{\alpha_2}\left\{D\nabla^2\nabla^2 w - N_{11}\left[\frac{1}{G_1}\frac{\partial}{\partial\alpha_1}\left(\frac{1}{G_1}\frac{\partial w}{\partial\alpha_1}\right)+\frac{1}{G_1G_2^2}\frac{\partial G_1}{\partial\alpha_2}\frac{\partial w}{\partial\alpha_2}\right]\right. \tag{30}$$

$$- N_{22}\left[\frac{1}{G_2}\frac{\partial}{\partial\alpha_2}\left(\frac{1}{G_2}\frac{\partial w}{\partial\alpha_2}\right)+\frac{1}{G_1^2G_2}\frac{\partial G_2}{\partial\alpha_1}\frac{\partial w}{\partial\alpha_1}\right]$$

$$- 2N_{12}\left[\frac{1}{G_2}\frac{\partial}{\partial\alpha_2}\left(\frac{1}{G_1}\frac{\partial w}{\partial\alpha_1}\right)-\frac{1}{G_1G_2^2}\frac{\partial G_2}{\partial\alpha_1}\frac{\partial w}{\partial\alpha_2}\right]$$

$$\left.- \rho h\left[\frac{1}{G_1}\frac{\partial^2 u}{\partial t^2}\frac{\partial w}{\partial\alpha_1}+\frac{1}{G_2}\frac{\partial^2 v}{\partial t^2}\frac{\partial w}{\partial\alpha_2}-\frac{\partial^2 w}{\partial t^2}\right]\right\}\delta w\, G_1G_2\, d\alpha_2\, d\alpha_1$$

$$+\int_{\alpha_2}\left\{Q_1+\frac{1}{G_2}\frac{\partial M_{12}}{\partial\alpha_2}+N_{11}\frac{1}{G_1}\frac{\partial w}{\partial\alpha_1}+N_{12}\frac{1}{G_2}\frac{\partial w}{\partial\alpha_2}\right\}\delta w\, G_2\Big|_{\alpha_1} d\alpha_2$$

$$-\int_{\alpha_2}\left\{\frac{1}{G_1}M_{11}\right\}\frac{\partial\delta w}{\partial\alpha_1}\, G_2\Big|_{\alpha_1} d\alpha_2 = 0 \quad ,$$

where

$$\nabla^2 = \frac{1}{G_1G_2}\left[\frac{\partial}{\partial\alpha_1}\left(\frac{G_2}{G_1}\frac{\partial}{\partial\alpha_1}\right)+\frac{\partial}{\partial\alpha_2}\left(\frac{G_1}{G_2}\frac{\partial}{\partial\alpha_2}\right)\right] \quad . \tag{31}$$

Equations (27) and (28) are the in-plane equations of motion for the plate. The expression in brackets under the double

integration sign in Equation (30), if set to zero, is the out-of-plane equation of motion. The expressions in brackets under the single integration signs in Equation (30), if set to zero, are the natural transverse boundary conditions for the plate. These conditions are not separated into three separate equations, however, but are left as one equation because of the method of solution that is to be used in a later section.

Stress Function

Equations (27) and (28) are the in-plane equations of motion for the plate. If it is assumed that in-plane inertia effects can be neglected, these equations become

$$\left.\begin{aligned} &\frac{\partial}{\partial\alpha_1}\left(G_2 N_{11}\right) - \frac{\partial G_2}{\partial\alpha_1} N_{22} + \frac{1}{G_1}\,\frac{\partial}{\partial\alpha_2}\left(G_1^2 N_{12}\right) = 0 \\ \text{and}\quad &\frac{\partial}{\partial\alpha_2}\left(G_1 N_{22}\right) - \frac{\partial G_1}{\partial\alpha_2} N_{11} + \frac{1}{G_2}\,\frac{\partial}{\partial\alpha_1}\left(G_2^2 N_{12}\right) = 0 \end{aligned}\right\} \quad (32)$$

This assumption is acceptable when the in-plane excitation frequency of the plate is not close to an in-plane natural frequency of the plate, References [13,14]. Equations (32) can be satisfied identically by representing the stress resultants in terms of a stress function $\phi(\alpha_1, \alpha_2, t)$ as

$$
\left.
\begin{aligned}
N_{11} &= \frac{1}{G_2}\,\frac{\partial}{\partial\alpha_2}\left(\frac{1}{G_2}\,\frac{\partial\phi}{\partial\alpha_2}\right) + \frac{1}{G_1^2 G_2}\,\frac{\partial G_2}{\partial\alpha_1}\,\frac{\partial\phi}{\partial\alpha_1}\,, \\
N_{22} &= \frac{1}{G_1}\,\frac{\partial}{\partial\alpha_1}\left(\frac{1}{G_1}\,\frac{\partial\phi}{\partial\alpha_1}\right) + \frac{1}{G_1 G_2^2}\,\frac{\partial G_1}{\partial\alpha_2}\,\frac{\partial\phi}{\partial\alpha_2}\,, \\
N_{12} &= -\frac{1}{G_1}\,\frac{\partial}{\partial\alpha_1}\left(\frac{1}{G_2}\,\frac{\partial\phi}{\partial\alpha_2}\right) + \frac{1}{G_1^2 G_2}\,\frac{\partial G_1}{\partial\alpha_2}\,\frac{\partial\phi}{\partial\alpha_1}\,.
\end{aligned}
\right\} \quad (33)
$$

These equations were obtained from Reference [15].

Compatibility Equation

It is possible to obtain a compatibility equation containing ϵ_{11}^0, ϵ_{22}^0, ϵ_{12}^0 and the displacement component w by eliminating the displacement components u and v from Equations (14). In Reference [16] the author presents a compatibility equation in curvilinear coordinates for the linear theory of thin elastic shells. Although Equations (14) are non-linear plate equations, Reference [16] was used as a guide in developing the following compatibility equation:

$$\frac{\partial}{\partial\alpha_2}\left\{\frac{1}{G_2}\left[\frac{\partial}{\partial\alpha_2}\left(G_1\epsilon^0_{11}\right) - \frac{\partial G_1}{\partial\alpha_2}\epsilon^0_{22} - \frac{\partial}{\partial\alpha_1}\left(G_2\,\epsilon^0_{12}\right)\right.\right.$$

$$\left.\left. - \frac{\partial G_2}{\partial\alpha_1}\epsilon^0_{12}\right]\right\} + \frac{\partial}{\partial\alpha_1}\left\{\frac{1}{G_1}\left[\frac{\partial}{\partial\alpha_1}\left(G_2\,\epsilon^0_{22}\right)\right.\right.$$

$$\left.\left. - \frac{\partial G_2}{\partial\alpha_1}\epsilon^0_{11} - \frac{\partial}{\partial\alpha_2}\left(G_1\,\epsilon^0_{12}\right) - \frac{\partial G_1}{\partial\alpha_2}\epsilon^0_{12}\right]\right\}$$

$$= \frac{1}{2}\,\frac{\partial}{\partial\alpha_2}\left\{\frac{1}{G_2}\left[\frac{\partial}{\partial\alpha_2}\left[\frac{1}{G_1}\left(\frac{\partial w}{\partial\alpha_1}\right)^2\right] - \frac{1}{G_2^2}\,\frac{\partial G_1}{\partial\alpha_2}\left(\frac{\partial w}{\partial\alpha_2}\right)^2\right.\right.$$

$$\left.\left. - \frac{\partial}{\partial\alpha_1}\left[\frac{1}{G_1}\,\frac{\partial w}{\partial\alpha_1}\,\frac{\partial w}{\partial\alpha_2}\right] - \frac{1}{G_1G_2}\,\frac{\partial G_2}{\partial\alpha_1}\,\frac{\partial w}{\partial\alpha_1}\,\frac{\partial w}{\partial\alpha_2}\right]\right\}$$

$$+ \frac{1}{2}\,\frac{\partial}{\partial\alpha_1}\left\{\frac{1}{G_1}\left[\frac{\partial}{\partial\alpha_1}\left[\frac{1}{G_2}\left(\frac{\partial w}{\partial\alpha_2}\right)^2\right] - \frac{1}{G_1^2}\,\frac{\partial G_2}{\partial\alpha_1}\left(\frac{\partial w}{\partial\alpha_1}\right)^2\right.\right.$$

$$\left.\left. - \frac{\partial}{\partial\alpha_2}\left[\frac{1}{G_2}\,\frac{\partial w}{\partial\alpha_1}\,\frac{\partial w}{\partial\alpha_2}\right] - \frac{1}{G_1G_2}\,\frac{\partial G_1}{\partial\alpha_2}\,\frac{\partial w}{\partial\alpha_1}\,\frac{\partial w}{\partial\alpha_2}\right]\right\}.$$

The compatibility equation can be expressed in terms of the stress function ϕ by using Equations (20) and (33). This equation is

$$\nabla^2\nabla^2\phi = \frac{Eh}{2}\ \frac{\partial}{\partial\alpha_2}\left\{\frac{1}{G_2}\left[\frac{\partial}{\partial\alpha_2}\left[\frac{1}{G_1}\left(\frac{\partial w}{\partial\alpha_1}\right)^2\right]\right.\right. \tag{34}$$

$$-\frac{1}{G_2^2}\ \frac{\partial G_1}{\partial\alpha_2}\left(\frac{\partial w}{\partial\alpha_2}\right)^2 - \frac{\partial}{\partial\alpha_1}\left[\frac{1}{G_1}\ \frac{\partial w}{\partial\alpha_1}\ \frac{\partial w}{\partial\alpha_2}\right]$$

$$\left.\left. -\frac{1}{G_1G_2}\ \frac{\partial G_2}{\partial\alpha_1}\ \frac{\partial w}{\partial\alpha_1}\ \frac{\partial w}{\partial\alpha_2}\right]\right\} + \frac{Eh}{2}\ \frac{\partial}{\partial\alpha_1}\left\{\frac{1}{G_1}\left[\frac{\partial}{\partial\alpha_1}\left[\frac{1}{G_2}\left(\frac{\partial w}{\partial\alpha_2}\right)^2\right]\right.\right.$$

$$-\frac{1}{G_1^2}\ \frac{\partial G_2}{\partial\alpha_1}\left(\frac{\partial w}{\partial\alpha_1}\right)^2 - \frac{\partial}{\partial\alpha_2}\left[\frac{1}{G_2}\ \frac{\partial w}{\partial\alpha_1}\ \frac{\partial w}{\partial\alpha_2}\right]$$

$$\left.\left. -\frac{1}{G_1G_2}\ \frac{\partial G_1}{\partial\alpha_2}\ \frac{\partial w}{\partial\alpha_1}\ \frac{\partial w}{\partial\alpha_2}\right]\right\}\ ,$$

where ∇^2 is given by Equation (31).

Setting the expression under the double integration sign in Equation (30) equal to zero, dropping the inertia terms and using the values of G_1 and G_2 equal to unity for Cartesian coordinates, gives one of the two well known Karman equations for moderately large deflections of plates. The second Karman equation is obtained from Equation (34) by setting the values of G_1 and G_2 equal to unity.

Dynamic Stability Equations

Consider a thin plate undergoing a steady-state, in-plane motion under the action of the boundary loading:

$$\left.\begin{aligned} \bar{N}_{11}(\alpha_2,t) &= \gamma\, \bar{N}^{S}_{11}(\alpha_2) + \beta\Psi(t)\, \bar{N}^{D}_{11}(\alpha_2) \\ \text{and} \quad \bar{N}_{12}(\alpha_2,t) &= \gamma\, \bar{N}^{S}_{12}(\alpha_2) + \beta\Psi(t)\, \bar{N}^{D}_{12}(\alpha_2)\ , \end{aligned}\right\} \quad (35)$$

on the outer boundary of the plate and

$$\bar{N}_{11} = 0 \quad \text{and} \quad \bar{N}_{12} = 0 \qquad (36)$$

on the inner boundary of the plate (Figure 5). The symbols γ and β

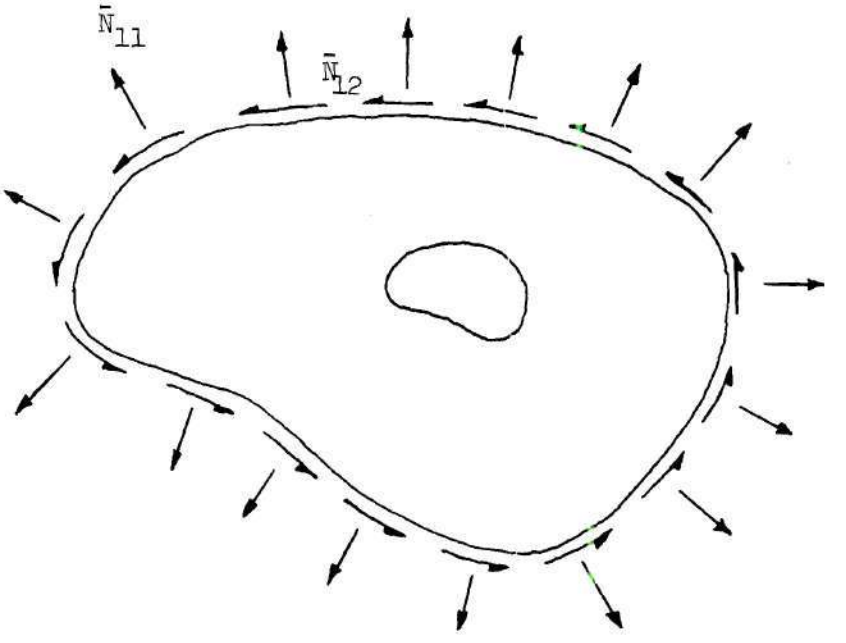

Figure 5. Loading on Plate

are loading parameters, $\bar{N}^S$ and $\bar{N}^D$ are normalized static and dynamic load distributions, and Ψ is a periodic function of time. Since the plate is experiencing plane motion, the motion is governed by the differential equation

$$\nabla^2 \nabla^2 \phi_o = 0 \tag{37}$$

which is obtained by substituting the value of w equal to zero into Equation (34). The zero subscript on ϕ indicates in-plane motion. The boundary conditions for this problem, Equations (35) and (36) can be expressed in terms of ϕ_o by using Equations (33). The solution of the problem posed can be written in the form

$$\left.\begin{aligned} N_{11}(\alpha_1,\alpha_2,t) &= \gamma\, N^S_{11}(\alpha_1,\alpha_2) + \beta\Psi(t)\, N^D_{11}(\alpha_1,\alpha_2) \\ N_{22}(\alpha_1,\alpha_2,t) &= \gamma\, N^S_{22}(\alpha_1,\alpha_2) + \beta\Psi(t)\, N^D_{22}(\alpha_1,\alpha_2) \\ \text{and} \quad N_{12}(\alpha_1,\alpha_2,t) &= \gamma\, N^2_{12}(\alpha_1,\alpha_2) + \beta\Psi(t)\, N^D_{12}(\alpha_1,\alpha_2) \end{aligned}\right\} \tag{38}$$

because the operator $\nabla^2 \nabla^2$ is linear and does not contain any operation with respect to the variable of time.

A small transverse disturbance can be applied to the plate in the form

$$w = w_0 + w_1 \ ,$$

where w_1 represents the disturbance. The plate was experiencing only in-plane motion before the disturbance was applied. Therefore, w_0 would be equal to zero and the above equation becomes

$$w = w_1 \ .$$

Due to the disturbance, the stresses in the plate change. This can be taken into account by letting $\phi = \phi_o + \phi_1$, where ϕ_1 represents the change in the stress distribution due to the disturbance.

For a small disturbance, ϕ_o can be considered to be much larger than ϕ_1. This implies that Equation (37) is satisfactory for determining the stress distribution in the plate. If w_1 or just w is expressed in series form as

$$w(\alpha_1, \alpha_2, t) = \sum_m^\infty \sum_n^\infty f_{mn}(t)\, \chi_{mn}(\alpha_1, \alpha_2) \tag{39}$$

then the variation of w is

$$\delta w = \sum_k^\infty \sum_\ell^\infty \frac{\partial w}{\delta f_{k\ell}}\, \delta f_{k\ell}$$

From Equation (39) $\partial w/\partial f_{k\ell} = \chi_{k\ell}$ and the above equation becomes

$$\delta w = \sum_k^\infty \sum_\ell^\infty \chi_{k\ell}\, \delta f_{k\ell} \tag{40}$$

after making this substitution. Equation (30) is the governing equation for motion in the transverse direction. Substituting Equation (38) and (40) into Equation (30) gives a doubly infinite set of equations for investigating the stability of thin plates expressing in-plane motion. These equations are

$$\sum_{m}^{\infty}\sum_{n}^{\infty}\left\{a_{k\ell mn}\ \frac{\partial^2 f_{mn}}{\partial t^2} + \left[b_{k\ell mn} - \gamma\ c_{k\ell mn} - \beta\Psi(t)\ d_{k\ell mn}\right] f_{mn}\right\} = 0 \tag{41}$$

where k ranges from m to infinity, ℓ ranges from n to infinity and

$$a_{k\ell mn} = \int_{\alpha_1}\int_{\alpha_2} \rho h\ \chi_{mn}\ \chi_{k\ell}\ G_1\ G_2\ d\alpha_2\ d\alpha_1 \tag{42}$$

$$b_{k\ell mn} = \int_{\alpha_1}\int_{\alpha_2} D\left(\nabla^2\ \nabla^2\ \chi_{mn}\right)\chi_{k\ell}\ G_1\ G_2\ d\alpha_2\ d\alpha_1$$

$$+ \int_{\alpha_2}\left(Q_1 + \frac{1}{G_2}\ \frac{\partial M_{12}}{\partial \alpha_2}\right)\chi_{k\ell}\ G_2 \Big|_{\alpha_1} d\alpha_2$$

$$- \int_{\alpha_2}\left(\frac{1}{G_1}\ M_{11}\right)\frac{\partial \chi_{k\ell}}{\partial \alpha_1}\ G_2 \Big|_{\alpha_1} d\alpha_2$$

$$c_{k\ell mn} = \int_{\alpha_1}\int_{\alpha_2} \Big\{ N^S_{11} \Big[\frac{1}{G_1} \frac{\partial}{\partial\alpha_1} \Big(\frac{1}{G_1} \frac{\partial \chi_{mn}}{\partial\alpha_1} \Big) + \frac{1}{G_1 G_2^2} \frac{\partial G_1}{\partial\alpha_2} \frac{\partial \chi_{mn}}{\partial\alpha_2} \Big]$$

$$+ N^S_{22} \Big[\frac{1}{G_2} \frac{\partial}{\partial\alpha_2} \Big(\frac{1}{G_2} \frac{\partial \chi_{mn}}{\partial\alpha_2} \Big) + \frac{1}{G_1^2 G_2} \frac{\partial G_2}{\partial\alpha_1} \frac{\partial \chi_{mn}}{\partial\alpha_1} \Big]$$

$$+ 2\, N^S_{12} \Big[\frac{1}{G_2} \frac{\partial}{\partial\alpha_2} \Big(\frac{1}{G_1} \frac{\partial \chi_{mn}}{\partial\alpha_1} \Big) - \frac{1}{G_1 G_2^2} \frac{\partial G_2}{\partial\alpha_1} \frac{\partial \chi_{mn}}{\partial\alpha_2} \Big] \Big\} \chi_{k\ell} G_1 G_2 d\alpha_2 d\alpha_1$$

$$- \int_{\alpha_2} \Big\{ N^S_{11} \frac{1}{G_1} \frac{\partial \chi_{mn}}{\partial\alpha_1} + N^S_{12} \frac{1}{G_2} \frac{\partial \chi_{mn}}{\partial\alpha_2} \Big\} \chi_{k\ell} G_2 \Big|_{\alpha_1} d\alpha_2$$

$$d_{k\ell mn} = \int_{\alpha_1}\int_{\alpha_2} \Big\{ N^D_{11} \Big[\frac{1}{G_1} \frac{\partial}{\partial\alpha_1} \Big(\frac{1}{G_1} \frac{\partial \chi_{mn}}{\partial\alpha_1} \Big) + \frac{1}{G_1 G_2^2} \frac{\partial G_1}{\partial\alpha_2} \frac{\partial \chi_{mn}}{\partial\alpha_2} \Big]$$

$$+ N^D_{22} \Big[\frac{1}{G_2} \frac{\partial}{\partial\alpha_2} \Big(\frac{1}{G_2} \frac{\partial \chi_{mn}}{\partial\alpha_2} \Big) + \frac{1}{G_1^2 G_2} \frac{\partial G_2}{\partial\alpha_1} \frac{\partial \chi_{mn}}{\partial\alpha_1} \Big]$$

$$+ 2\, N^D_{12} \Big[\frac{1}{G_2} \frac{\partial}{\partial\alpha_2} \Big(\frac{1}{G_1} \frac{\partial \chi_{mn}}{\partial\alpha_1} \Big) - \frac{1}{G_1 G_2^2} \frac{\partial G_2}{\partial\alpha_1} \frac{\partial \chi_{mn}}{\partial\alpha_2} \Big] \Big\} \chi_{k\ell} G_1 G_2 d\alpha_2 d\alpha_1$$

$$- \int_{\alpha_2} \Big\{ N^D_{11} \frac{1}{G_1} \frac{\partial \chi_{mn}}{\partial\alpha_1} + N^D_{12} \frac{1}{G_2} \frac{\partial \chi_{mn}}{\partial\alpha_2} \Big\} \chi_{k\ell} G_2 \Big|_{\alpha_1} d\alpha_2 \,.$$

Equation (41) can also be expressed in matrix form as

$$\Big[A\Big] \Big\{ \frac{\partial^2 f}{\partial t^2} \Big\} + \Big[B\Big] \Big\{f\Big\} - \gamma \Big[C\Big] \Big\{f\Big\} - \beta\Psi(t) \Big[D\Big] \Big\{f\Big\} = \Big\{0\Big\} \qquad (43)$$

The matrices [A], [B], [C] and [D] are composed of the elements $a_{k\ell mn}$, $b_{k\ell mn}$, $c_{k\ell mn}$ and $d_{k\ell mn}$ respectively. The matrices $\{f\}$ and $\{0\}$ are column matrices composed of the elements f_{mn} and zeros respectively.

The governing equations for the following problems can be obtained by setting various combinations of the matrices equal to zero in Equation (43):

(1) static stability of a thin plate,
([A] = [D] = [0]),

(2) natural vibration of a thin plate without in-plane loading
([C] = [D] = [0]),

(3) natural vibration of a thin plate with in-plane loading
([D] = [0]).

CHAPTER III

ANALYTICAL INVESTIGATION

Introduction

In the previous chapter a general development of the governing equations for dynamic stability was presented. By use of the appropriate curvilinear coordinate system, these equations can be used to analyze problems involving a variety of boundary shapes. In this chapter the general equations are specialized to develop a detailed analysis of a specific problem.

Consider the rectangular plate with a centrally located circular hole in the center (Figure 6). When the plate is loaded by uniformly

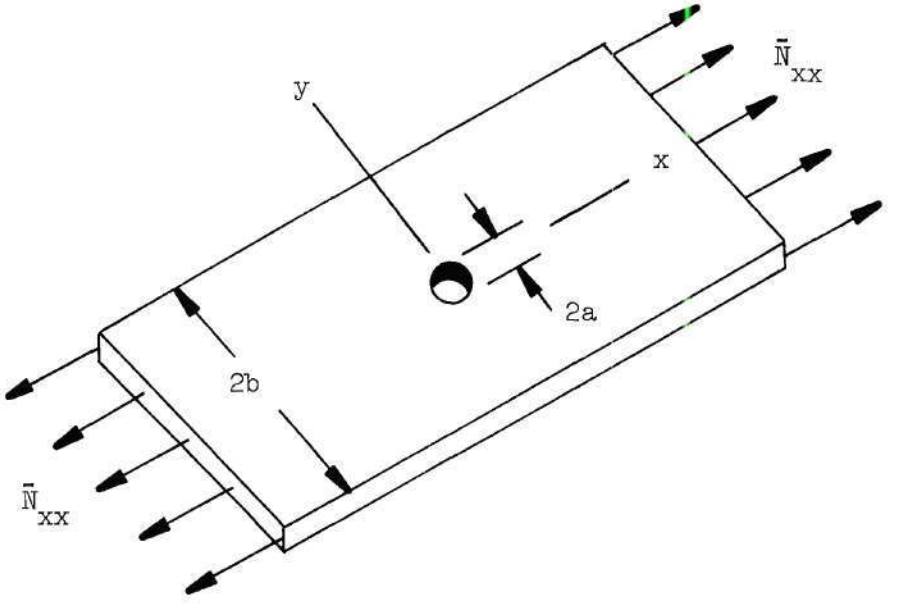

Figure 6. Rectangular Plate with Circular Hole

distributed tensile forces along two opposite edges, a non-uniform stress distribution is developed in the plate. The determination of the stress field when all of the outer boundaries extend to infinity and the plate material is linear elastic is a classic problem. The solution is found in most books on the theory of elasticity [17]. The stress field has three important characteristics:

(1) there are stresses in the plate that are larger than the applied external stress

(2) the effect of the circular opening is local in nature

(3) there exists a region of compressive stresses in the vicinity of the hole.

The first characteristic of the stress field is the one which has been given the most attention by investigators. The emphasis of the problem is usually on evaluating the stress concentration which is the ratio of the maximum tangential stress along the inner boundary to the uniformly applied external stress. The important feature of the stress field for the title problem, however, is not the stress concentration, but the fact that a region of compression exists in the vicinity of the inner boundary. Due to this region of compression, it is conceivable for the region to experience an instability in the plane equilibrium configuration. This, of course, depends on the parameters of the problem which are the magnitude of the loading, the material properties of the plate and the dimensions of the plate and the hole. Thus, the possibility of a local static stability problem exists. By keeping the load uniform along the edge of the

plate but allowing the magnitude of the load to vary with time, a local dynamic stability problem also is possible.

In-Plane Stress Distribution

The plate under consideration has a rectangular outer boundary and a circular inner boundary. The diameter of the hole is assumed to be small compared to the length and width of the plate. To simplify the problem, the rectangular outer boundary is changed to a circular boundary with a radius that is large compared to the radius of the circular inner boundary (Figure 7). The validity of this change is

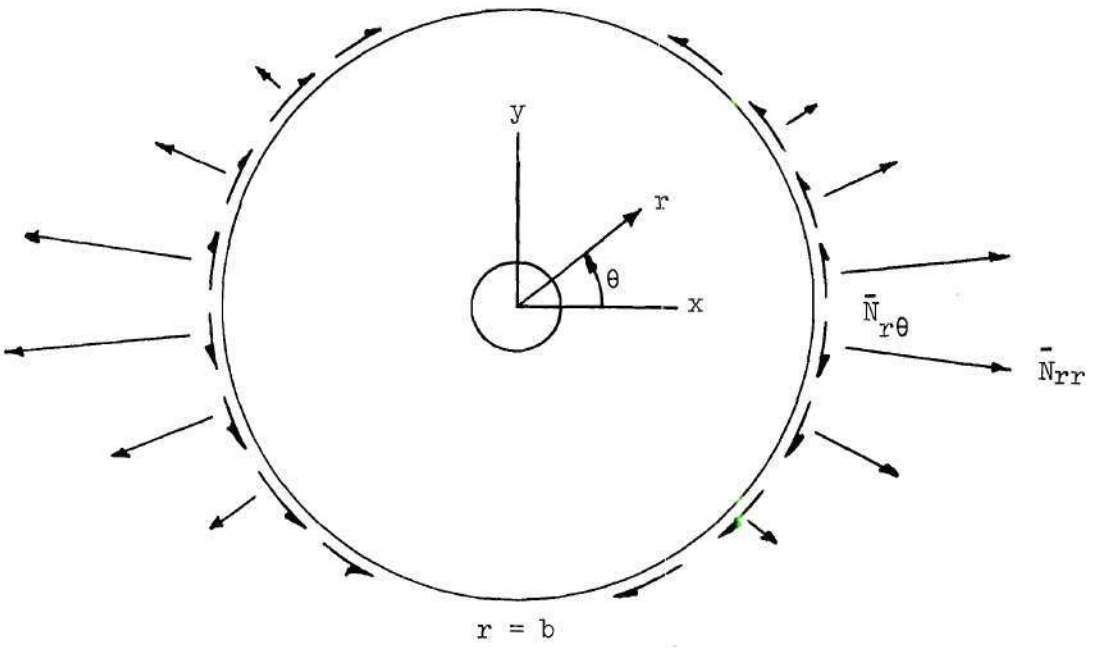

Figure 7. Circular Plate with Circular Hole

justified by the fact that the out-of-plane deflection of the plate is confined locally to a region near the inner boundary of the plate.

Changing the outer boundary of the plate, makes it necessary to replace the outer boundary loading $\bar{N}_{xx}$ with an equipollent loading expressed in terms of $\bar{N}_{xx}$ and θ as

$$\bar{N}_{rr} = \frac{1}{2} \bar{N}_{xx} \left(1 + \cos 2\theta\right)$$

and

$$\bar{N}_{r\theta} = - \frac{1}{2} \bar{N}_{xx} \sin 2\theta \quad .$$

$\bar{N}_{xx}$ can be expressed in terms of the loading parameters γ and β by using the first of Equations (35) of Chapter II. This expression is

$$\bar{N}_{xx}(y,t) = \gamma \bar{N}^{S}_{xx}(y) + \beta \Psi(t) \bar{N}^{D}_{xx}(y) \quad .$$

The static and dynamic components of the boundary loading $\bar{N}_{xx}$ are taken to be uniform for this particular problem. Therefore, $\bar{N}^{S}_{xx}$ and $\bar{N}^{D}_{xx}$ are constant along the boundary and can be set equal to unity. The equation for $\bar{N}_{xx}$ becomes

$$\bar{N}_{xx}(t) = \gamma + \beta \Psi(t).$$

Substituting this expression for $\bar{N}_{xx}$ into the above expressions for $\bar{N}_{rr}$ and $\bar{N}_{r\theta}$ gives the dynamic loading,

$$\left.\begin{aligned} \bar{N}_{rr} &= \frac{1}{2}\left[\gamma + \beta\, \Psi(t)\right]\left[1 + \cos 2\theta\right] \\ \text{and} \qquad \bar{N}_{r\theta} &= -\frac{1}{2}\left[\gamma + \beta\, \Psi(t)\right] \sin 2\theta \end{aligned}\right\} \quad (1)$$

on the circular outer boundary of the plate shown in Figure 7. The loading on the circular inner boundary is

$$\bar{N}_{rr} = 0 \quad \text{and} \quad \bar{N}_{r\theta} = 0 \; . \qquad (2)$$

Equations (1) and (2) are the boundary conditions for the problem of determining the in-plane stress distribution.

The governing differential equation in curvilinear coordinates for the determination of the in-plane stress distribution is Equation (37) of Chapter II where the differential operator is defined by Equation (31) of Chapter II. In order to convert this equation to polar coordinates it is necessary to use the appropriate values of G_1 and G_2 in the differential operator. These values are obtained from Equations (1) of Chapter II with the transformation equations from Cartesian to polar coordinates which are

$$x = r \cos\theta \quad \text{and} \quad y = r \sin\theta \; .$$

The values of G_1 and G_2 for polar coordinates are

$$G_1 = 1 \quad \text{and} \quad G_2 = r. \qquad (3)$$

Using Equations (3) the governing differential equation in polar

coordinates for determining the in-plane stress distribution is

$$\nabla^2 \nabla^2 \phi_0 = 0 \quad , \tag{4}$$

where

$$\nabla^2 = \frac{\partial^2}{\partial r^2} + \frac{1}{r} \frac{\partial}{\partial r} + \frac{1}{r^2} \frac{\partial^2}{\partial \theta^2} \quad . \tag{5}$$

The solution of Equation (4) with boundary conditions given by Equations (1) and (2) is presented in Reference [17] for a plate in which the outer boundary is located at infinity. The stress distribution which satisfies the governing differential equation and boundary conditions is

$$\left.\begin{aligned} N_{rr} &= \gamma N^S_{rr} + \beta \Psi(t) N^D_{rr} \\ N_{\theta\theta} &= \gamma N^S_{\theta\theta} + \beta \Psi(t) N^D_{\theta\theta} \\ \text{and} \quad N_{r\theta} &= \gamma N^S_{r\theta} + \beta \Psi(t) N^D_{r\theta} \end{aligned}\right\} \tag{6}$$

where N^S_{rr}, $N^S_{\theta\theta}$, $N^S_{r\theta}$, N^D_{rr}, $N^D_{\theta\theta}$ and $N^D_{r\theta}$ are given by the equations

$$N^S_{rr} = N^D_{rr} = \frac{1}{2}\left(1 - \frac{a^2}{r^2}\right) + \frac{1}{2}\left(1 - \frac{4a^2}{r^2} + \frac{3a^4}{r^4}\right)\cos 2\theta$$

$$N^S_{\theta\theta} = N^D_{\theta\theta} = \frac{1}{2}\left(1 + \frac{a^2}{r^2}\right) - \frac{1}{2}\left(1 + \frac{3a^4}{r^4}\right)\cos 2\theta \qquad (7)$$

and $$N^S_{r\theta} = N^D_{r\theta} = -\frac{1}{2}\left(1 + \frac{2a^2}{r^2} - \frac{3a^4}{r^4}\right)\sin 2\theta$$

This stress distribution is also a good approximation to the stress distribution for a plate with a finite outer boundary as long as the outer boundary radius is large compared to the inner boundary radius.

Local Static Stability Problem

As stated in the preceding chapter, the governing equations for dynamic stability can be reduced to the governing equations for static stability by setting certain quantities in the equations equal to zero. The static stability problem plays an important part in the dynamic stability problem because any solution of the latter problem must contain the solution of the former problem. Therefore, before proceeding to the more general problem, the local static stability problem is examined.

D. A. Pellett [18] apparently was the first person to conduct a mathematical investigation of the local static stability of an infinite plate with a circular opening subjected to a uniaxial tension loading. He used the Rayleigh Ritz method described in Reference [19]. Because of the local nature of the stability problem, Pellett chose

$$w(r,\theta) = \sum_{m=1}^{M} \sum_{n=0}^{N} f_{mn}\, r^{-m} \left[1 + S_{mn}/r + T_{mn}/r^2\right]\left[\sin n\theta + \cos n\theta\right] \qquad (8)$$

for his assumed deflection function. This function satisfies the geometric boundary conditions of zero slope and deflection at infinity where the plate should be flat. Substituting the deflection function into the equations for zero shear and moment on the circular inner boundary, he obtained two equations from which the unknown constants S_{mn} and T_{mn} were determined. Thus, he was able to satisfy all of the boundary conditions. Substituting w and the static in-plane stress distribution into the energy functional, integrating, and then differentiating with respect to each unknown coefficient f_{mn}, he obtained four sets of linear algebraic equations. Four sets of equations were obtained because the unknown coefficients uncoupled due to the orthogonality of the trigonometric functions in the integrations. Each set of equations were classified by the symmetry or anti-symmetry of the deflection function as follows:

(1) symmetric about the x axis and symmetric about the y axis ($\cos n\theta$, $n = 0, 2, 4, \ldots$)

(2) symmetric about the x axis and anti-symmetric about the y axis ($\cos n\theta$, $n = 1, 3, 5, \ldots$)

(3) anti-symmetric about the x axis and symmetric about the y axis ($\sin n\theta$, $n = 1, 3, 5, \ldots$)

(4) anti-symmetric about the x axis and anti-symmetric about the y axis ($\sin n\theta$, $n = 2, 4, 6, \ldots$)

The equations for each group formed a generalized eigenvalue problem of the form

$$\left[B\right]\left\{f\right\} - K_L\left[C\right]\left\{f\right\} = \left\{0\right\} \quad , \tag{9}$$

where K_L is the loading coefficient $\left(K_L = \gamma a^2/D\right)$, $\left[B\right]$ is a symmetric and positive definite matrix, $\left[C\right]$ is a symmetric matrix, $\left\{f\right\}$ is a column matrix of the unknown coefficients, D is the bending stiffness, and "a" is the hole radius. The bending stiffness and the square of the hole radius can be factored out from each coefficient in the B matrix, but Poisson's ratio appears in a complicated manner. It must be given a specific value in order to calculate the coefficients. Using a matrix similarity transformation (Appendix B) he reduced the generalized eigenvalue problem to the special eigenvalue problem in which the matrices are symmetric and K_L appears only in the diagonal elements. By using the Jacobi method [20] to solve this eigenvalue problem, he obtained both positive and negative eigenvalues. The lowest positive eigenvalue corresponds to the smallest tensile load which produces local buckling around the hole. Pellett's result for the local critical load can be expressed as

$$N_{cr} = K_L^1 \, D/a^2 \quad ,$$

where K_L^1 represents the smallest positive eigenvalues calculated from Equations (9). Because of slow convergence of the approximate solution to the exact solution, Pellett used a least squares procedure to extra-

polate to a value of K_L^1 for an infinite number of terms. For a value of $\nu = .3$, the lowest positive value of K_L^1 he calculated using this procedure was 85.54. The mode which corresponded to this eigenvalue was symmetric about both the x and the y axes.

Shortly after Pellett had finished his work on the problem, R. G. Costello [21] discovered two errors in Pellett's formulation of the problem. He corrected the mistakes and computed a new value of K_L^1 using Pellett's computer programs. The value he calculated for K_L^1 is 18.72. In examining Costello's work, an error is found in his expression for the strain energy due to bending which would cause his result to be incorrect also. He had a factor of $(2 - \nu)$ in his equation when the factor should have been $2(1 - \nu)$. The symbol ν is Poisson's ratio. The incorrect factor would cause the value of K_L^1 to be lower than the value of K_L^1 calculated by the correct factor.

Another indication that Costello's value of K_L^1 is incorrect is an experimental and analytical investigation made by P. K. Datta [22]. Datta calculated the local critical loads for several plates which contained elliptical openings. The limiting case in his investigation was the plate with a circular hole. The results he obtained along with the result obtained by using Costello's formula for the critical load are shown in Figure 8. As can be seen, an extrapolation of Datta's curve indicates the higher value of K_L^1 than that calculated by Costello.

In light of these observations, the remaining portion of this section is devoted to the investigation of the local static stability of the plate containing a circular hole when subjected to uniaxial tension. The equations necessary for examining this problem are given

All dimensions in inches

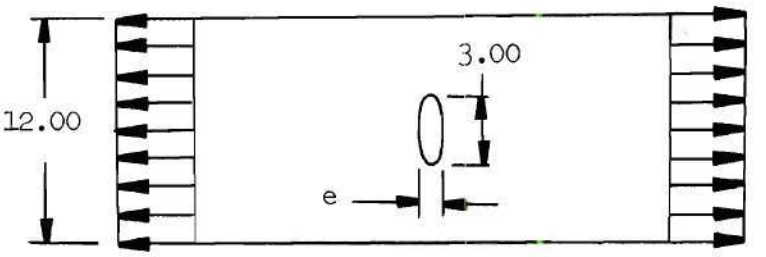

h = 0.025

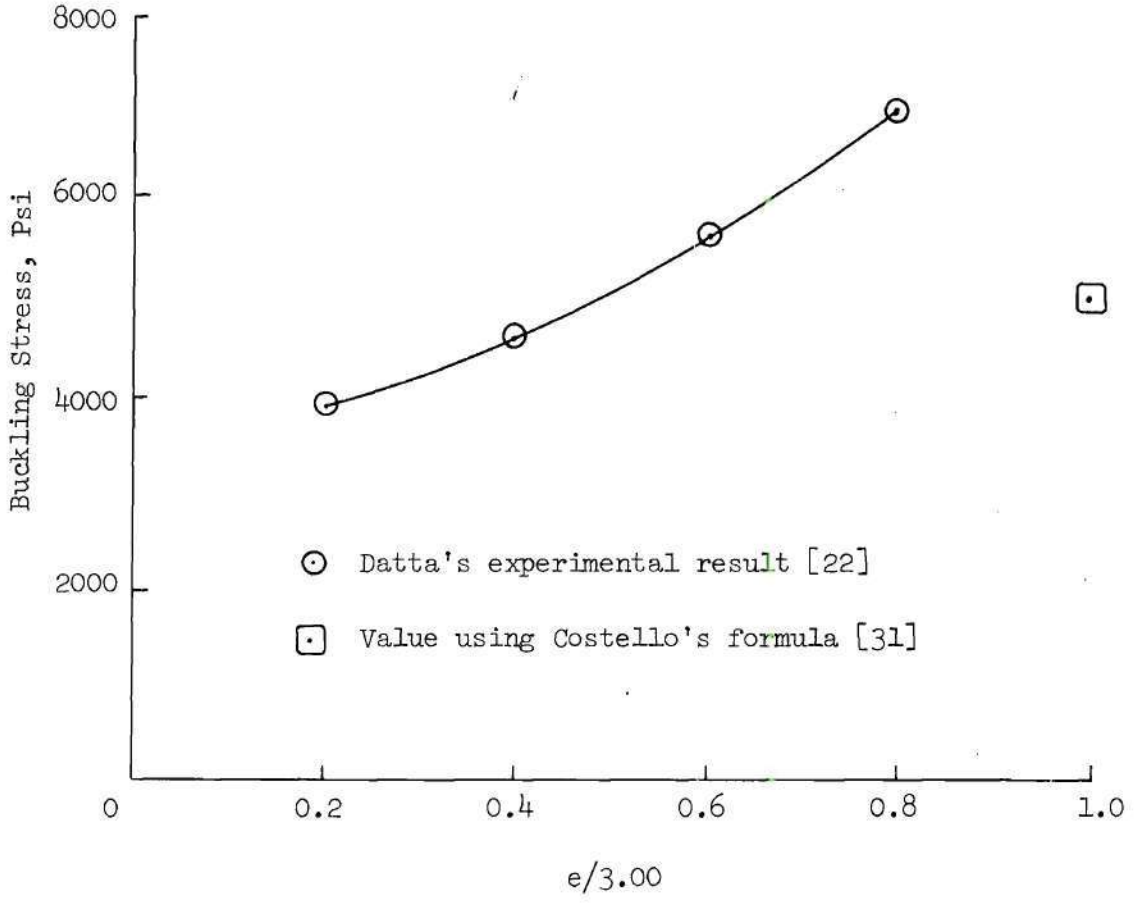

Figure 8. Buckling Stress versus Hole Shape

by Equations (41) of Chapter II with the coefficients $a_{k\ell mn}$ and $d_{k\ell mn}$ set equal to zero. The equations are

$$\sum_{m}^{\infty}\sum_{n}^{\infty}\left(b_{k\ell mn} - \gamma\, c_{k\ell mn}\right) f_{mn} = 0 \,, \tag{10}$$

where $k = m, \ldots, \infty$ and $\ell = n, \ldots, \infty$

The coefficients $b_{k\ell mn}$ and $c_{k\ell mn}$ are calculated from the second and third of Equations (42) of Chapter II. For polar coordinates ($G_1 = 1$ and $G_2 = r$) these two equations become

$$\left.\begin{aligned} b_{k\ell mn} = {} & \int_{a}^{\infty}\int_{0}^{2\pi} D\left(\nabla^2\nabla^2\chi_{mn}\right)\chi_{k\ell}\; r\, d\theta\, dr \\ & + \int_{0}^{2\pi}\left(Q_r + \frac{1}{r}\frac{\partial M_{r\theta}}{\partial\theta}\right)\chi_{k\ell}\; r \Big|_{a}^{\infty} d\theta \\ & - \int_{0}^{2\pi} M_{rr}\frac{\partial\chi_{k\ell}}{\partial r}\; r \Big|_{a}^{\infty} d\theta \,, \end{aligned}\right\} \tag{11}$$

and

$$\left.\begin{aligned} c_{k\ell mn} = {} & \int_{a}^{\infty}\int_{0}^{2\pi}\left\{N^{S}_{rr}\frac{\partial^2\chi_{mn}}{\partial r^2} + N_{\theta\theta}\left[\frac{1}{r}\frac{\partial\chi_{mn}}{\partial r}\right.\right. \\ & \left.\left. + \frac{1}{r^2}\frac{\partial^2\chi_{mn}}{\partial\theta^2}\right] + 2N_{r\theta}\left[\frac{1}{r}\frac{\partial^2\chi_{mn}}{\partial r\partial\theta}\right.\right. \end{aligned}\right\}$$

$$- \frac{1}{r^2} \frac{\partial \chi_{mn}}{\partial \theta} \Big] \Big\} \chi_{k\ell} \, r \, d\theta \, dr$$

$$- \int_0^{2\pi} \left\{ N^S_{rr} \frac{\partial \chi_{mn}}{\partial r} + N^S_{r\theta} \frac{1}{r} \frac{\partial \chi_{mn}}{\partial \theta} \right\} \chi_{k\ell} \, r \Big|_a^\infty \, d\theta \, .$$

The terms $\left(Q_r + \frac{1}{r} \frac{\partial M_{r\theta}}{\partial \theta} \right)$ and M_{rr} can be expressed in terms of χ_{mn} by using Equations (15), (21) and (26) of Chapter II with G_1 equal to one and G_2 equal to r. The resulting expressions are

$$\left(Q_r + \frac{1}{r} \frac{\partial M_{r\theta}}{\partial \theta} \right) = - D \left[\frac{\partial^3 \chi_{mn}}{\partial r^3} + \frac{1}{r} \frac{\partial^2 \chi_{mn}}{\partial r^2} - \frac{1}{r^2} \frac{\partial \chi_{mn}}{\partial r} \right.$$

$$\left. - \frac{(3-\nu)}{r^3} \frac{\partial^2 \chi_{mn}}{\partial \theta^2} + \frac{(2-\nu)}{r^2} \frac{\partial^3 \chi_{mn}}{\partial r \partial \theta^2} \right]$$

and

$$M_{rr} = - D \left[\frac{\partial^2 \chi_{mn}}{\partial r^2} + \frac{\nu}{r} \frac{\partial \chi_{mn}}{\partial r} + \frac{\nu}{r^2} \frac{\partial^2 \chi_{mn}}{\partial \theta^2} \right] .$$

The differential operator ∇^2 is given in Equation (5) of this chapter and the stress resultants N^S_{rr}, $N^S_{\theta\theta}$ and $N^S_{r\theta}$ are given by Equations (7) of this chapter.

The coefficients for Equations (10) can now be calculated by selecting suitable approximation function $\chi_{mn}(r, \theta)$, substituting these functions into the expressions for $b_{k\ell mn}$ and $c_{k\ell mn}$ and then

integrating. Knowing the coefficients, the solution to the static stability problem is obtained by finding the non-trivial solutions of the algebraic homogeneous Equations (10). Instead of using the Jacobi method which was used by Pellett and Costello, the values of K_L^1 obtained in this section were calculated by the method described in Appendix C.

The first approximation functions selected to investigate the problem were

$$\chi_{mn}(r,\theta) = e^{-mr/a} \cos n\theta \,, \qquad \begin{matrix} m = 1, 2, 3, \ldots \\ n = 0, 2, 4, \ldots \end{matrix} \quad .$$

The exponential function was chosen in order to satisfy the geometric boundary conditions at infinity. The cosine function with even integer powers was chosen because this investigation is concerned with only the lowest positive eigenvalues, and as Pellett and Costello found in their investigations, these particular trigonometric functions produce that value. The natural boundary conditions on the inner circular boundary do not have to be satisfied by the approximation function χ_{mn} because they are satisfied in an average sense by the governing equations for the problem. The integration for the coefficients could not be evaluated exactly and the numerical values of the exponential integrals (Appendix D) were used. The trigonometric identities in Appendix E were also used in obtaining the coefficients. When the coefficients, $b_{kl\,mn}$ and $c_{kl\,mn}$, which were accurate to four significant figures were used, the values of K_L^1 in Table 1 were obtained.

Table 1. Values of K_L^1 Using $e^{-mr/a} \cos n\theta$

Values of m and n	Lowest Positive Eigenvalue, K_L^1
m = 1 n = 0	No positive value of K_L^1
m = 1, 2 n = 0, 2	No positive value of K_L^1
m = 1, 2, 3 n = 0, 2, 4	$K_L^1 = 67.19$
m = 1, 2, 3, 4 n = 0, 2, 4, 6	$K_L^1 = 7.57$

These results are surprising in view of the fact that Costello's value of K_L^1, which was previously reasoned as being low, is 18.72. G. S. Mikhlin stated in his book, Approximate Methods for the Solution of Differential and Integral Equations [23]:

> The approximate solution given by the energy method approaches the exact solution as the number of terms for the approximation increases. This is true if the approximate solution is computed without error, but in practice, as a rule, the situation is different. The approximate solution is determined from the energy method, which is constructed and solved with some error. The error, which we assume to be small, is not very important if the number of terms used in the approximation is small, i.e., if the energy method is used to find only a crude approximation. If however, it is desired to construct a more exact approximation, it is necessary to use higher-order approximations, and here the errors accumulated during computation of the matrices for the energy method, as well as in solving this system, can reach appreciable proportions. This raises the problem of determining whether the energy method is stable with respect to this kind of small error.

Mikhlin stated that this type of error can be minimized by using orthogonal approximation functions. Another way to minimize the error would be to increase the accuracy in the computations. Choosing the latter approach, the accuracy of the coefficients was increased from four to seven significant figures and the values of K_L^1 were re-calculated. These values appear in Table 2. A comparison of the results in Table 1 and Table 2 leads one to believe that there does exist a computational instability in the energy method.

Table 2. Values of K_L^1 Using $e^{-mr/a} \cos n\theta$ and Increasing the Accuracy

Values of m and n	Lowest Positive Eigenvalue, K_L^1
m = 1 n = 0	No positive value of K_L^1
m = 1, 2 n = 0, 2	No positive value of K_L^1
m = 1, 2, 3 n = 0, 2, 4	$K_L^1 = 67.67$
m = 1, 2, 3, 4 n = 0, 2, 4, 6	$K_L^1 = 45.17$
m = 1, 2, 3, 4, 5 n = 0, 2, 4, 5, 8	$K_L^1 = 42.84$

Upon discovering that this type of situation exists in the problem, the approximation functions

$$\chi_{mn}(r,\theta) = (a/r)^m \cos n\theta \quad , \quad \begin{matrix} m = 2, 3, 4, \ldots \\ n = 0, 2, 4, \ldots \end{matrix}$$

were adopted. The graphs of these functions when n is equal to zero and m is equal to two, three and four are shown in Figure 9. Unlike the other approximation functions which could not be integrated exactly, these functions can be integrated exactly. This means that the coefficients $b_{k\ell mn}$ and $c_{k\ell mn}$ can be calculated from exact algebraic equations instead of algebraic equations which contain approximate values of the exponential integrals. Using coefficients which were accurate to sixteen significant figures, the values of K_L^1 in Table 3 were obtained.

Table 3. Values of K_L^1 Using $(a/r)^m \cos n\theta$

Values of m and n	Lowest Positive Eigenvalue, K_L^1
m = 2 n = 0	No positive value of K_L^1
m = 2, 3 m = 0, 2	No positive value of K_L^1
m = 2, 3, 4 n = 0, 2, 4	$K_L^1 = 66.96$
m = 2, 3, 4, 5 n = 0, 2, 4, 6	$K_L^1 = 43.74$
m = 2, 3, 4, 5, 6 n = 0, 2, 4, 6, 8	$K_L^1 = 40.79$
m = 2, 3, 4, 5, 6, 7 n = 0, 2, 4, 6, 8, 10	$K_L^1 = 39.83$

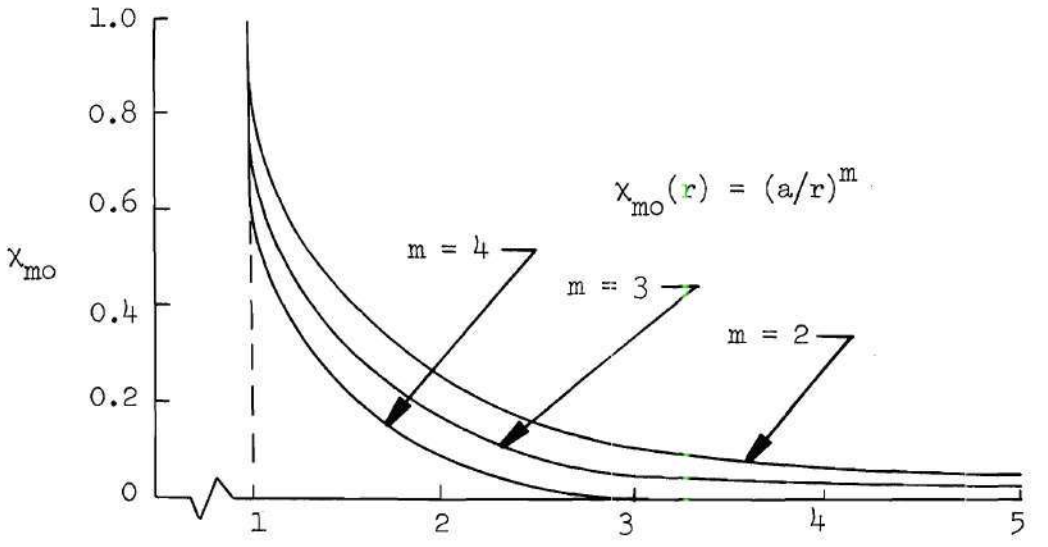

Figure 9. Plot of Approximation Functions

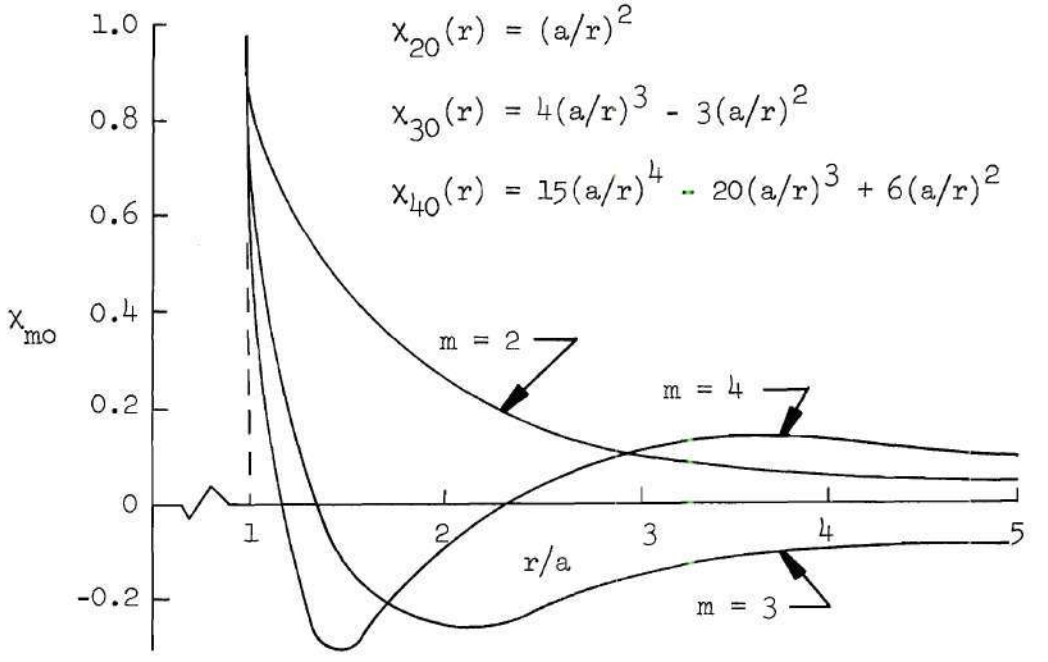

Figure 10. Plot of Orthogonalized Approximation Functions

It can be seen from Tables 2 and 3 that convergence appears to be slow.

A third set of approximation functions was tried. These functions were constructed using the Gram-Schmidt orthogonalization process. The first three of these functions are

$$\chi_{2n} = \left[(a/r)^2\right] \cos n\,\theta$$

$$\chi_{3n} = \left[4\,(a/r)^3 - 3\,(a/r)^2\right] \cos n\,\theta$$

and

$$\chi_{4n} = \left[15(a/r)^4 - 20(a/r)^3 + 6\,(a/r)^2\right] \cos n\,\theta$$

The graphs of these three functions when n is equal to zero are shown in Figure 10. Each function of r in an approximation function χ_{mn} is orthogonal to all of the other functions of r in the other approximation functions. The interval of orthogonalization extends from $r = a$ to infinity. Using sixteen significant figures, the values of K_L^1 for these functions are the same as those listed in Table 3. Since the orthogonized set of functions should provide the best accuracy for a given number of significant figures, it can, therefore, be concluded that the results of Table 3 are accurate. If a greater number of approximation functions were used, there would ultimately be a difference between the methods of computation.

In order to have an additional check of the method used in computing the eigenvalues, the method used by Pellett and Costello to calculate their eigenvalues was adopted. This method made use of a similarity transformation (Appendix B) and a Jacobi procedure. The

values of K_L^1 using this method were within one percent of those listed in Table 3.

The lowest value obtained for K_L^1 in Table 3 is 39.93. Thirty-six approximation functions were used to get this result. For the same number of terms Costello's value of K_L^1 is 19.05.

From the preceding analytical investigations, the following conclusions are made:

(1) Costello's value of K_L^1 is not correct.

(2) There is a computational instability in the particular energy method that was used.[1]

(3) For all approximation functions investigated convergence is slow.

Natural Vibration Problem

This section is concerned with the natural vibration of a plate with concentric circular inner and outer boundaries. A constant in-plane loading given by Equations (1) with $\Psi(t)$ equal to zero is applied on the outer boundary. The plate and loading are the same as discussed in the previous section except that the outer boundary of the plate is considered to be located at a finite distance from the center of the plate. This distance, however, is assumed to be large compared to the distance to the inner boundary, so that the stress distribution for the

---

[1] The energy method used in this investigation is called the Galerkin method. If another approximation method had been used, the computational instability may not have occurred.

infinite plate can be used. This problem is selected for two specific reasons:

(1) The problem illustrates how the general dynamic stability equations can be reduced to the equations necessary to analyze the natural vibration problem.

(2) The problem furnishes more information about the local static stability problem treated in the previous section.

The equations necessary to examine the problem are given by Equations (41) of Chapter II with the coefficients $d_{k\ell mn}$ set equal to zero. These equations are

$$\sum_{m}^{\infty}\sum_{n}^{\infty}\left[a_{k\ell mn}\frac{\partial^2 f_{mn}}{\partial t^2}+\left(b_{k\ell mn}-\gamma\, c_{k\ell mn}\right) f_{mn}\right]=0 \tag{12}$$

where $k = m, \ldots \infty$ and $\ell = n, \ldots \infty$.
Substituting the values of $G_1 = 1$ and $G_2 = r$ for polar coordinates into the first of Equations (42) of Chapter II, the expression

$$a_{k\ell mn}=\int_{a}^{b}\int_{o}^{2\pi}\rho h\, \chi_{mn}\, \chi_{k\ell}\, r\, d\theta\, dr \tag{13}$$

is obtained for the coefficients $a_{k\ell mn}$. The coefficients $b_{k\ell mn}$ and $c_{k\ell mn}$ are calculated from Equations (11) of the last section with the integration in the r direction extending from the inner boundary ($r = a$) to the outer boundary ($r = b$) instead of from the inner

boundary to infinity.

By using the approximation functions

$$\chi_{mn}(r,\theta) = \left[(r/b) - 1\right]^2 \left(a/r\right)^m \left[1 + S_{mn}(a/r) + T_{mn}(a/r)^2\right] \cos n\theta \ ,$$

all of the boundary conditions can be satisfied. The term $\left[(r/b)-1\right]^2$ satisfies the geometric boundary conditions of zero slope and deflection on the outer boundary. The constants S_{mn} and T_{mn} can be chosen so that the natural boundary conditions of zero shear and moment are satisfied on the inner boundary. Since the plate's outer boundary is finite, m can take on both positive and negative integer values. For convenience, the parameter ξ is introduced as the ratio of the outer boundary radius to the inner boundary radius,

$$\xi = b/a \ .$$

Using the parameter, the approximation functions becomes

$$\chi_{mn}(r,\theta) = \left[\frac{1}{\xi}(r/a) - 1\right]^2 \left(a/r\right)^m \left[1 + S_{mn}(a/r) + T_{mn}(a/r)^2\right] \cos n\theta$$

When these functions are used to calculate the coefficients $a_{k\ell mn}$, $b_{k\ell mn}$ and $c_{k\ell mn}$, the density ρ, the thickness h, the bending stiffness D and the square of the hole radius a^2 can be factored out; but the boundary ratio ξ and Poisson's ratio ν can not be. These quantities must be given specific values in order to calculate

the coefficients.

In matrix form Equations (12) are

$$a^2 \rho h \left[A\right] \left\{\frac{\partial^2 f}{\partial t^2}\right\} + D/a^2 \left[B\right] \left\{f\right\} - \gamma \left[C\right] \left\{f\right\} = \left\{0\right\}$$

If it is assumed that the plate experiences simple harmonic motion of the form

$$\left\{f\right\} = \left\{q\right\} e^{i\omega t}$$

the matrix equation becomes

$$- \omega^2 a^2 \rho h \left[A\right] \left\{q\right\} + D/a^2 \left[B\right] \left\{q\right\} - \gamma \left[C\right] \left\{q\right\} = \left\{0\right\} \quad .$$

Multiplying each term in this equation by a^2/D, the equation can be written as

$$- \left(K_F\right)^2 \left[A\right] \left\{q\right\} + \left[B\right] \left\{q\right\} - K_L \left[C\right] \left\{q\right\} = \left\{0\right\} \quad ,$$

where K_F is the frequency coefficient

$$K_F = \omega \, a^2 \sqrt{\rho h/D} \qquad (14)$$

and K_L is the buckling coefficient previously defined as $K_L = \gamma a^2/D$. By specifying a value of K_L, the smallest eigenvalue K_F^1 can be obtained by using the method of matrix iteration [24]. This method could not be used in obtaining the lowest positive eigenvalue in the static stability problem because the method converges to one over the smallest eigenvalue, and for the infinite plate, the smallest eigenvalue is zero. Knowing the value of K_F^1, the lowest natural frequency is given by

$$\omega_N = K_F^1 \sqrt{D/\rho h}\ /a^2$$

This equation is obtained by solving Equation (14) for the frequency ω.

For a fixed number of approximation functions, outer to inner boundary ratio and Poisson ratio, values of K_L were chosen and each corresponding eigenvalue problem was solved for the critical frequency coefficient K_F^1. A curve was then plotted in the K_F^1 - K_L plane. For a value of $\xi = 10$ and $\nu = .3$, the results obtained are shown in Figure 11. Table 4 gives the values of m and n for the approximation functions that were used to obtain each curve in Figure 11. The effect on K_F^1 of increasing the outer to inner boundary from $\xi = 10$ to $\xi = 50$ is shown in Figure 12. As was expected, the frequency decreases for an increase in ξ.

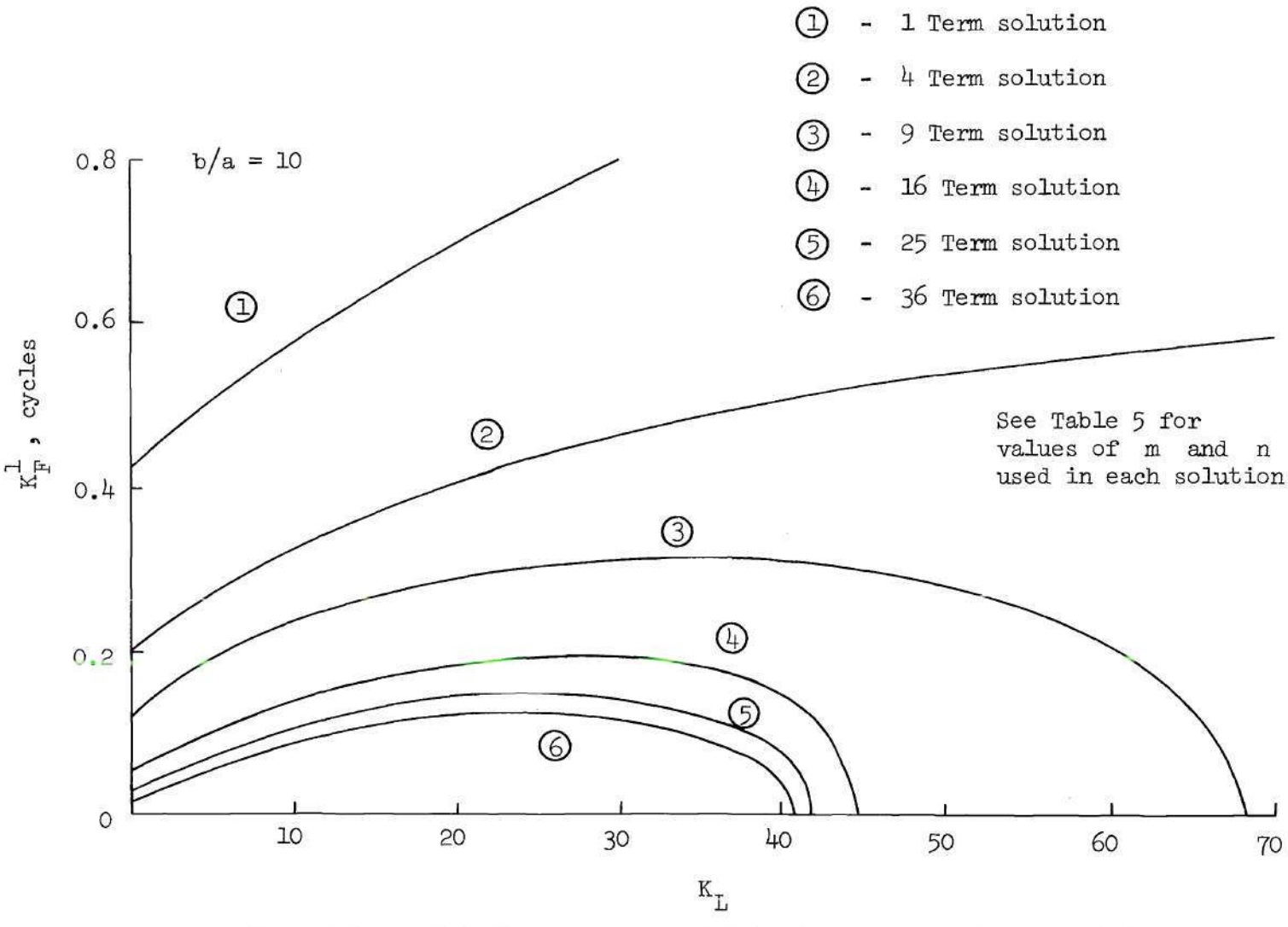

Figure 11. Critical Frequency Coefficient versus Loading Coefficient

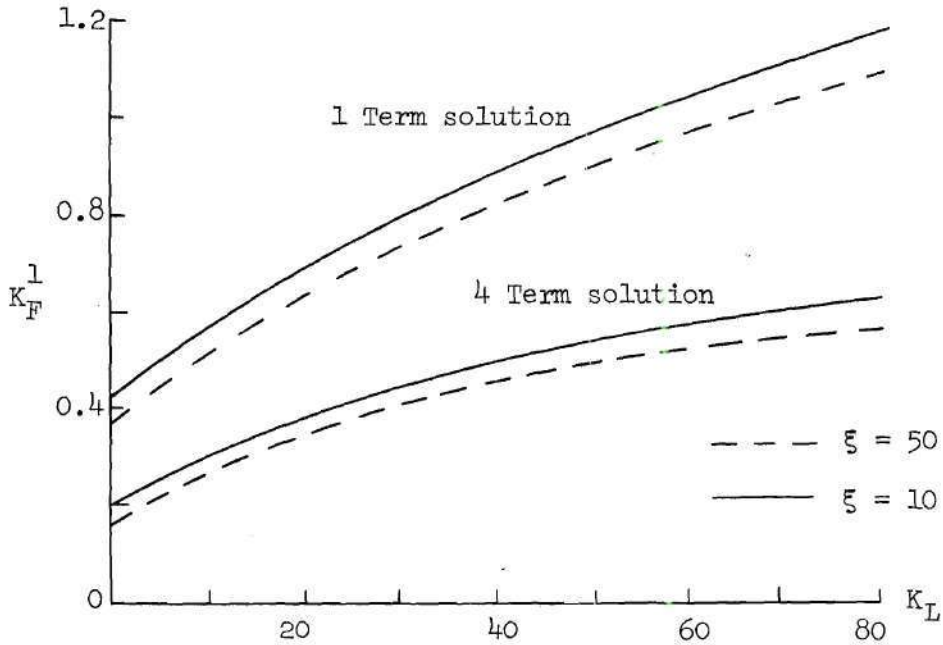

Figure 12(a). Effect on K_F^1 of Increasing $\xi = b/a$

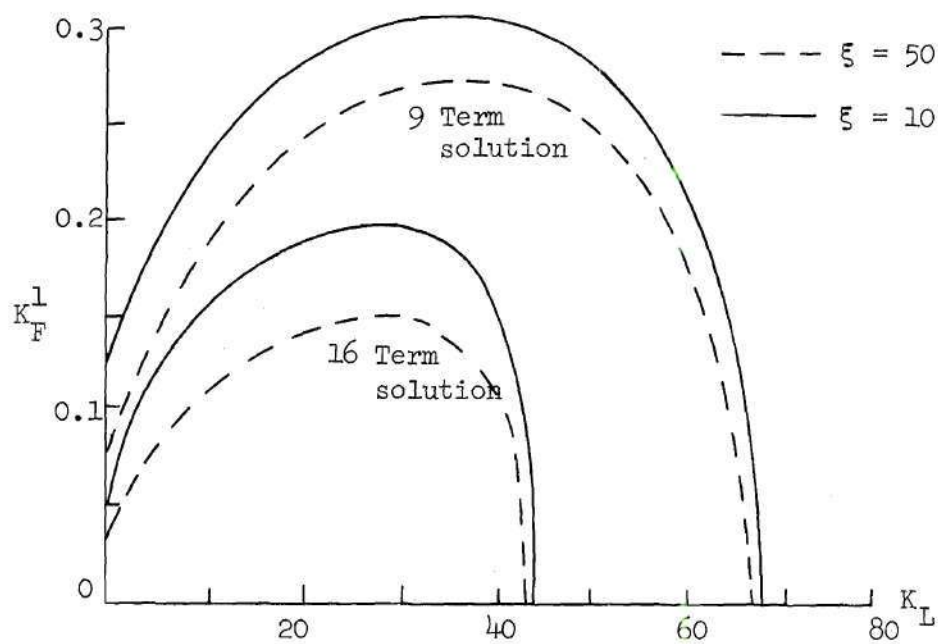

Figure 12(b) Effect of K_F^1 of Increasing $\xi = b/a$

Table 4. Values of m and n for Number of Approximation Functions Used

x	No of Terms	m	n
①	1	4	0
②	4	4,5	0,2
③	9	4,5,6	0,2,4
④	16	3,4,5,6	0,2,4,6
⑤	25	2,3,4,5,6	0,2,4,6,8
⑥	36	1,2,3,4,5,6	0,2,4,6,8,10

The value of K_L when the frequency is equal to zero ($K_F^1 = 0$) is the tensile buckling load K_L^1 for this problem. For the same number of terms, these values (Figure 11) are close to the values of K_L^1 in Table 3 of the last section. The values of K_L^1 should not agree exactly because one plate is large while the other is infinite. Also slightly different approximation function were used in each analysis. For the plate with $\xi = 10$, the value of K_L^1 for the 36 term solution is 40.50. For the plate with $\xi = 50$, the value of K_L^1 for the 36 term solution is 39.50. An increase in the value of from 50 to 100 did not produce any change in the value of $K_L^1 = 39.50$.

Based on Costello's value of K_L^1 for thirty-six terms ($K_L^1 = 19.05$) and his extrapolated value of K_L^1 for an infinite number of terms ($K_L^1 = 18.72$), the improvement was approximately 1.8 percent. Applying

this improvement to the value of $K_L^1 = 39.50$ gives a value for K_L^1 of 38.82.

The buckling mode shape corresponding to $K_L^1 = 39.50$ was computed and plotted in Figure 13 for the following cases:

(1) At $r = a$ for $0 \leq \theta \leq \pi/2$

(2) At $\theta = 0$ for $a \leq r \leq 50a$

and (3) At $\theta = \pi/2$ for $a \leq r \leq 50a$

The curves are normalized with respect to the deflection at the point $r = a$ and $\theta = 0$.

Dynamic Stability Problem

The investigations in the two previous sections were concerned with static stability and natural vibration of a plate. These subjects are special cases of the more general field of dynamic stability. This section deals with the dynamic stability problem for the plate described in the preceding section.

Since the phenomonon of local dynamic stability has never before been shown to exist, it was felt that an experimental rather than an analytical investigation would be the more effective means of establishing existence of the phenomonon.

In view of the exploratory nature of the investigation a detailed analytical solution to the problem was not developed. An outline of the method of solution which would be necessary for the class of problems which are of interest here is, however, presented in this section.

The governing equations for dynamic stability are Equations (43)

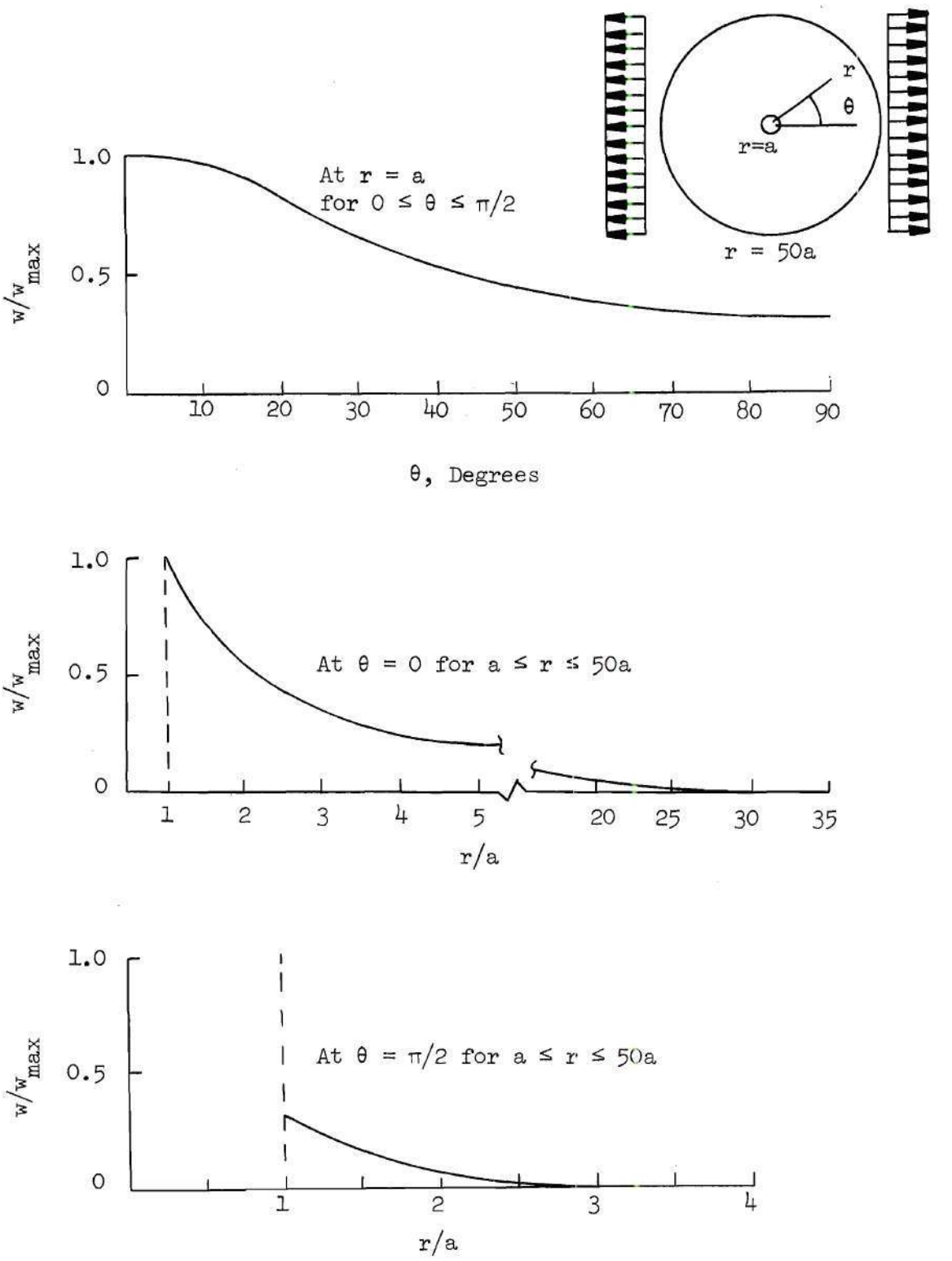

Figure 13. Mode Shape for $K_L^1 = 39.50$

of Chapter II. If $\Psi(t)$ is defined as

$$\Psi(t) = \cos \lambda t$$

the governing equations become

$$\left[A\right]\left\{\frac{d^2f}{dt^2}\right\} + \left[B\right]\left\{f\right\} - \gamma\left[C\right]\left\{f\right\} - \beta \cos \lambda t \left[D\right]\left\{f\right\} = \left\{0\right\} \qquad (15)$$

For the finite plate discussed in the previous two sections, the coefficients in the A, B and C matrices would be obtained from Equation (13) and Equations (11) with the upper limit on the integration in the r direction being b instead of infinity. The coefficients for the D matrix would be identical to the coefficients in the C matrix because it was previously stated that the static and dynamic loading distributions on the outer boundary of the plate have the same form. All the matrices in Equation (15) are symmetric. The matrices A and B are positive definite.

The solution to the problem involves finding the regions of stability and instability in parameter space (for this particular problem, parameter space is the γ, β and λ space). If the function $\Psi(t)$ is a periodic function with period T, the boundaries that separate these regions from one another are obtained by determining the conditions under which the differential equations governing the problem have periodic solutions of period T and 2T [25]. Therefore, since the cos λt is a periodic function of period $2\pi/\lambda$, the boundaries of the regions are obtained by finding the solutions of Equations (15)

which are periodic with period $2\pi/\lambda$ and $4\pi/\lambda$. The equations for determining the existence of solutions to the governing equations with period $4\pi/\lambda$ are obtained by substituting the Fourier series

$$\{f\} = \sum_{k=1,3}^{\infty} \{p\}_k \sin(k\lambda/2)t + \sum_{k=1,3}^{\infty} \{q\}_k \cos(k\lambda/2)t \tag{16}$$

into Equations (15) and setting the coefficients of $\sin(k\lambda/2)t$ and $\cos(k\lambda/2)t$ equal to zero. The coefficients $\{p\}_k$ and $\{q\}_k$ are time independent constants. Similarly, the equations for determining the existence of solutions to the governing equations with period $2\pi/\lambda$ are obtained by substituting the Fourier series

$$\{f\} = \sum_{k=2,4}^{\infty} \{p\}_k \sin(\lambda k/2)t + \sum_{k=2,4}^{\infty} \{q\}_k \cos(\lambda k/2)t \tag{17}$$

into Equations (15) and setting the coefficients of $\sin(k\lambda/2)t$ and $\cos(k\lambda/2)t$ equal to zero. An approximate expression for the boundaries of the principal region of instability is obtained by substituting only the first term in the Fourier series for $\{f\}$ given in Equation (16) into the governing equations and comparing coefficients of the trigonometric functions [26]. If this is done the following equations are obtained:

$$-\lambda^2/4 [A] + [B] - \gamma [C] \pm \beta/2 [D] = \{0\} \tag{18}$$

A boundary point for the principal region of instability can now be calculated by fixing two of the parameters γ and β and solving the resulting eigenvalue problem for the other parameter. By continually repeating this procedure, the boundaries of the principal instability region can be obtained.

Before concluding this section, an important characteristic of dynamic stability is derived. This is a relationship between the natural frequency ω_N of a plate with pre-load and the frequency λ at which the plate is being dynamically excited.

If the amplitude of excitation is small, that is, β is vanishingly small, Equations (18) for dynamic stability becomes

$$- \lambda^2/4 \left[A\right] + \left[B\right] - \gamma \left[C\right] = \left\{0\right\} \tag{19}$$

The natural vibration problem would be governed by Equations (15) with the D matrix equal to zero. Assuming simple harmonic motion the governing equations for the natural vibration problem are

$$- \omega^2 \left[A\right] + \left[B\right] - \gamma \left[C\right] = \left\{0\right\} \tag{20}$$

Comparing Equations (19) and (20) it can be seen that the natural frequency ω_N and the excitation frequency λ are related by the ratio

$$\omega / \lambda = 1/2 \quad .$$

Actually it can be shown [26] that by taking all the terms in the Fourier series, Equations (16) and (17), the natural frequency is related to the excitation frequency by the ratios.

$$\omega_N/\lambda = k/2 \ ,$$

where $k = 1, 2, 3, \ldots, \infty$. This indicates that the natural frequency and excitation frequency are related by the ratios 0.5, 1.0, 1.5, 2.0, etc.

CHAPTER IV

EXPERIMENTAL INVESTIGATION

Introduction

In the previous chapter, the analytical investigations of a thin tensioned sheet with a circular hole were presented. However, no conclusions were reached regarding the existence of local dynamic stability. This chapter describes an experimental investigation that was performed in order to provide information on this behavior.

Description of Testing Fixture and Specimens

The testing fixture shown in Figure 14 was designed and built especially for conducting the experiments described in this section. The base of the fixture is reinforced concrete and is isolated from the floor by four large springs. The vertical members are steel I beams. These beams are connected together at the top by a steel cross-over member which is used to house the loading assembly. The loading essembly is capable of applying a mean load to the specimen. The specimen was attached to the loading assembly by a pin connection. A horizontal spring was used to fasten the bottom end of the specimen. This connection was made by bolting two angle sections to the spring and connecting the angles to the specimen by means of a pin. The horizontal spring was designed so that only a small portion of the variable load from the shaker was transmitted to the I-beams.

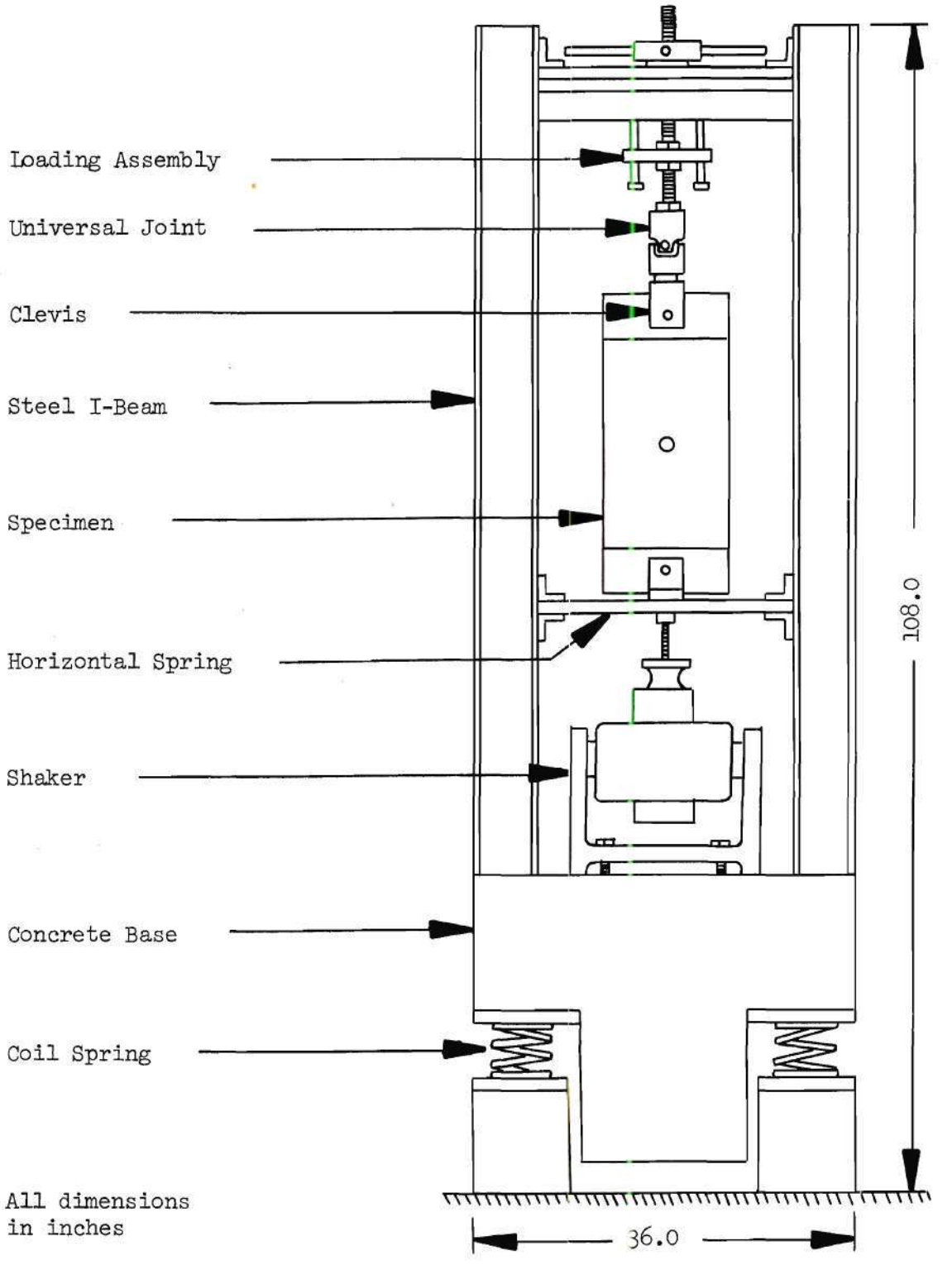

Figure 14. Testing Fixture

The first specimen used in the experiments was a rectangular sheet with a circular hole (Figure 15(a)). This specimen was made from 0.020 inch thick sheet of aluminum alloy 2024-T3. End plates made from 0.375 inch thick bar stock of aluminum alloy 2024-T4 were bonded on both faces of the sheet with room temperature curing epoxy. Two dowel pins were used at each end to insure proper alignment of the end plates on the sheet. The centrally located circular hole had a radius of 0.60 inch.

The second specimen used in the experiments was a rectangular sheet with an elliptic hole (Figure 15(b)). This specimen was made from 0.025 inch thick sheet of the aluminum alloy, Alclad 2024-T3. End plates similar to the ones used on the sheet with a circular hole were used on this specimen also. The elliptic hole was made in the specimen by using a numerically controlled milling machine which produced hole contours which were within 0.005 inch of the specified dimensions. The major axis of the elliptic hole was 3.00 inches and the minor axis was 0.60 inch.

Procedure and Results of Natural Frequency Investigation

Experiments were conducted to find the natural frequency of the sheet specimens for different values of applied tensile load. The following paragraphs describe the test procedure used and the data obtained.

Each specimen was placed in the testing fixture and a mean load was applied by turning the screw at the top of the fixture. The mean load was measured by connecting back to back strain gages (gages were

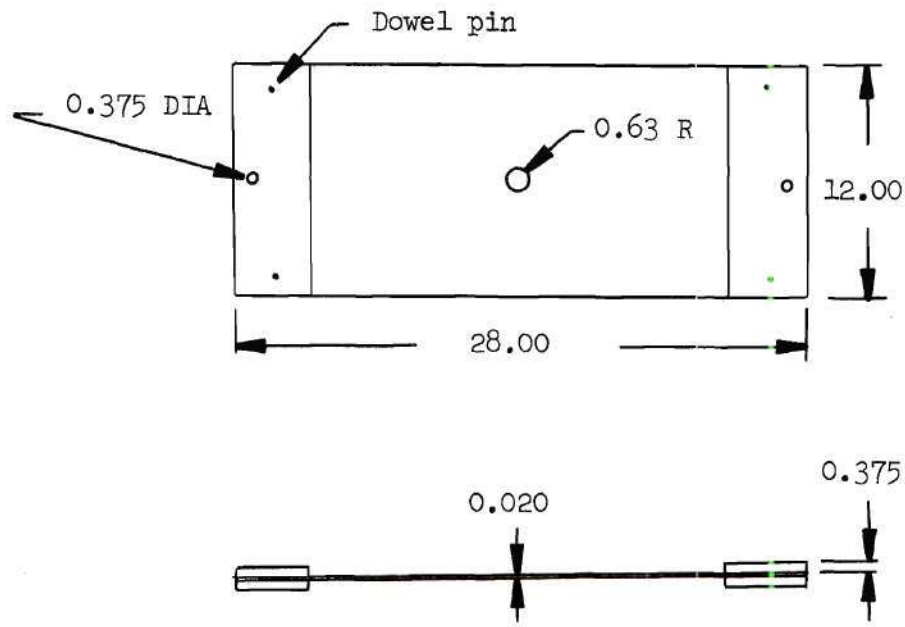

Figure 15(a). Specimen with Circular Hole

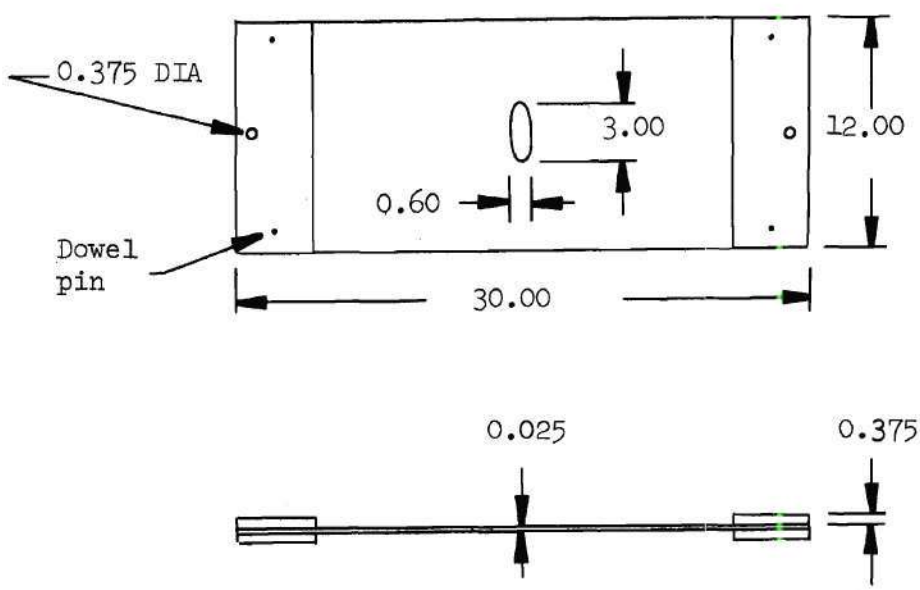

Figure 15(b). Specimen with Elliptic Hole

All dimensions in inches

located at point A on the specimen in Figure 16) to a bridge that measured the sum of the two gage outputs. The sum of the two gage outputs provides a measure of the mid-surface strain. After the mean load was applied, an electrodynamic shaker was connected to the bottom of the horizontal spring. An audio oscillator in conjunction with a power amplifier was used to generate the input signal to the shaker. When the shaker was operating, the dynamic response of the free edge of the holes was measured by back to back strain gages (gages were located at point B on the specimen in Figure 16). These gages were connected to another bridge which measured the difference of the two gage outputs. The difference of the two gage outputs provided a measure of the local bending strain. The strain gages had a sensitivity factor of 2.09 and a resistance of 120 Ohms. A description of the instruments that were used in these experiments is presented in Table 5.

Table 5. Instrument Specifications

Instrument	Model	Manufacturer
Electronic Shaker	C11	M. B. Electronics
Amplifier	104	Accudata
SR-4 Strain Indicator	Type N	Baldwin-Lima-Hamilton
SR-4 Strain Indicator	Type 20	Baldwin-Lima-Hamilton
Oscillator	T112531	M. B. Electronics
Oscillator	209A	Hewlett Packard
Tracking Filter	SD101B	Spectral Dynamics Corp.
Oscilloscope	Type 502A	Tektronix
Attenuator	350D	Hewlett Packard
RMS Voltmeter	3400A	Hewlett Packard

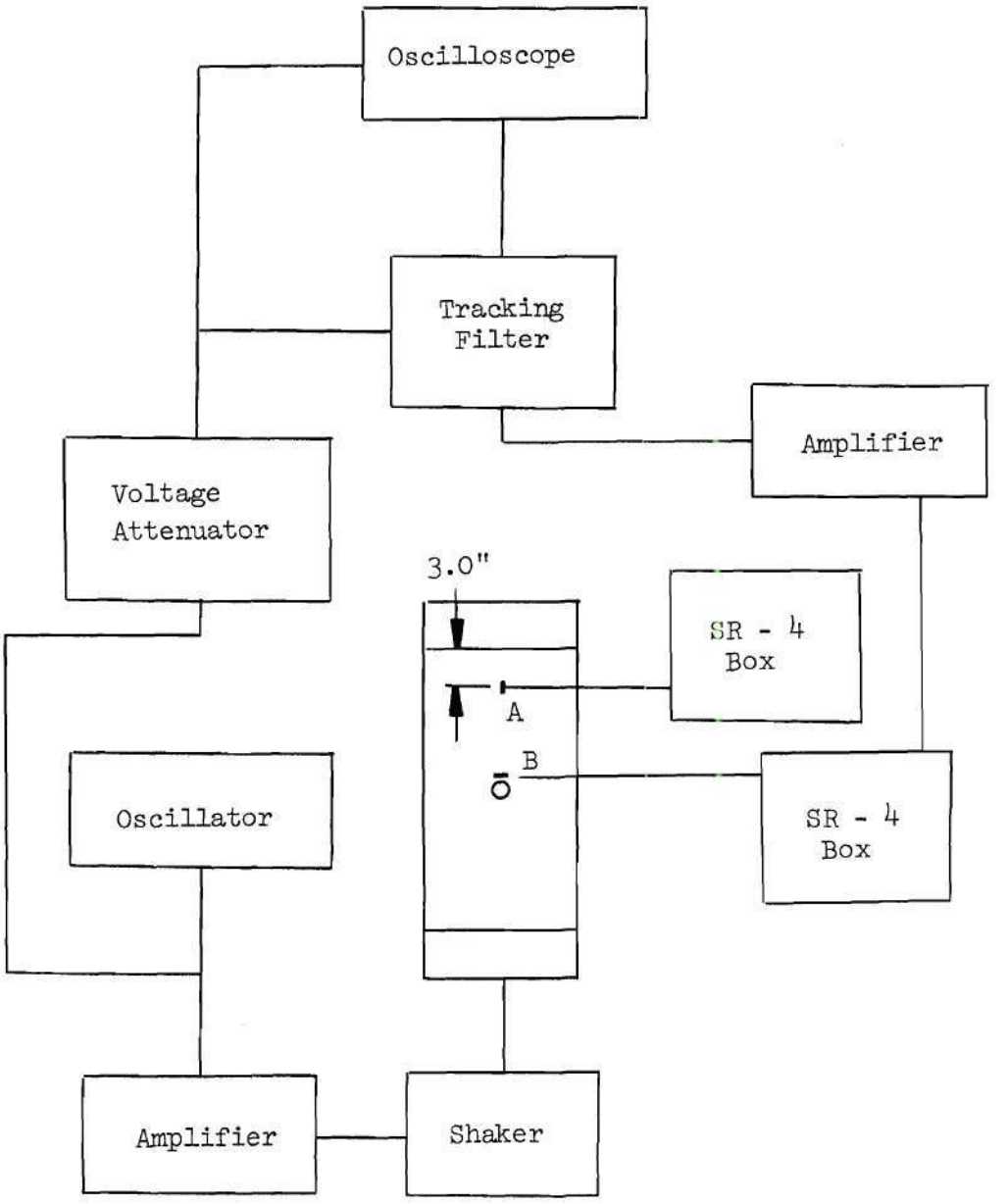

Figure 16. Schematic Diagram for Natural Frequency Experiment

The natural frequency of vibration at different tensile loads was detected by use of an oscilloscope. A schematic diagram of the test facility is shown in Figure 16. The exciting force signal, after passing through a voltage attenuator to reduce its strength, was fed into the horizontal input of the oscilloscope. The response (dynamic bending strain) signal was amplified to increase its strength and was fed into a tracking filter. The tracking filter which utilized a 1-1/2 Hertz filter was tuned by the exciting force signal. The response signal was then fed into the vertical input of the oscilloscope. The force versus response trace on the oscilloscope screen was an ellipse as shown in Figure 17. The change in sign of the in-phase component of response was used as an indication of the transition through the natural frequency.

The lowest natural frequency of the specimens was found by varying the frequency on the oscillator and observing the oscilloscope. The data obtained in this experiment for both specimens are shown in Figure 18. The natural frequency versus load curve for the specimen containing the elliptic hole shows that for increasing loads in the region from E to F in the figure the frequency decreases. This is due to the influence of the local region of compressive stress near the hole. Although a tensile load applied to the specimen with the circular hole produces a local region of compressive stress near the opening, the influence of the compressive region on the natural frequency of the specimen does not appear to be as great as in the other specimen. In the region from C to D in Figure 18(a), an increase in load produces an increase in frequency. The specimen with the elliptic hole was

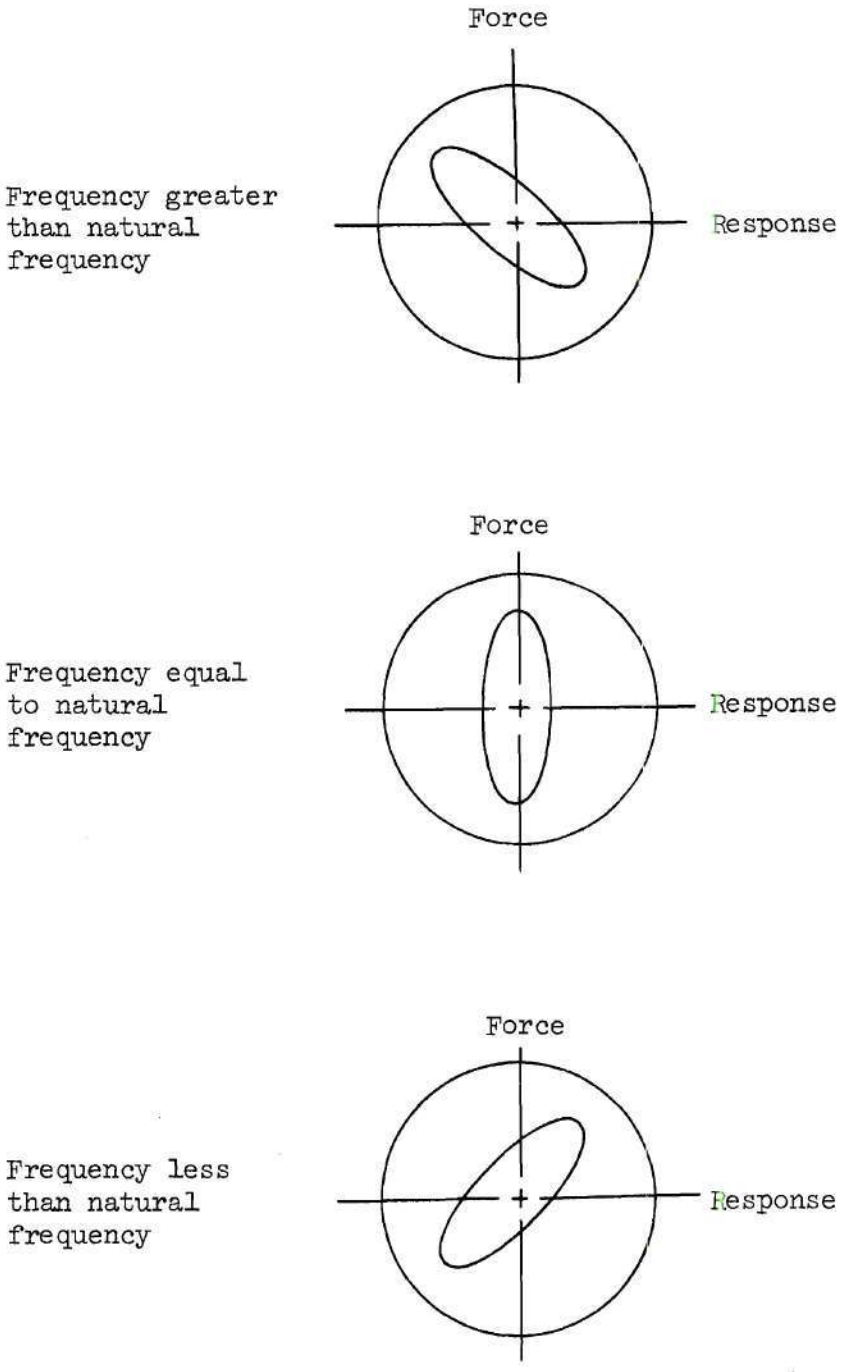

Figure 17. Force versus Response Plot on the Oscilloscope Screen

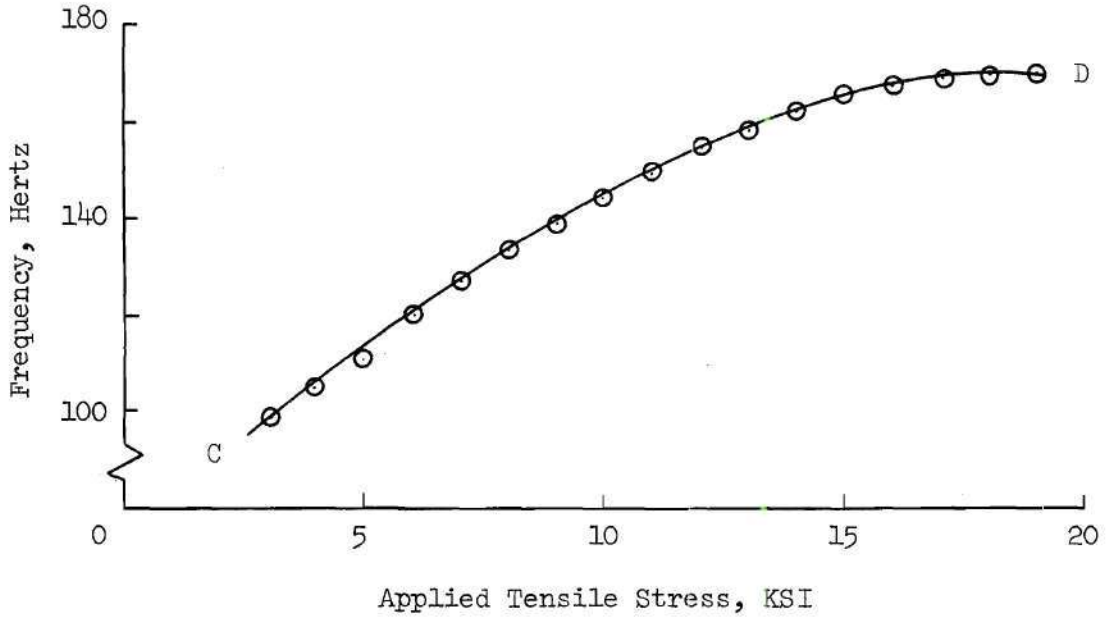

Figure 18(a). Natural Frequency versus Applied Stress Curve for Specimen with Circular Hole

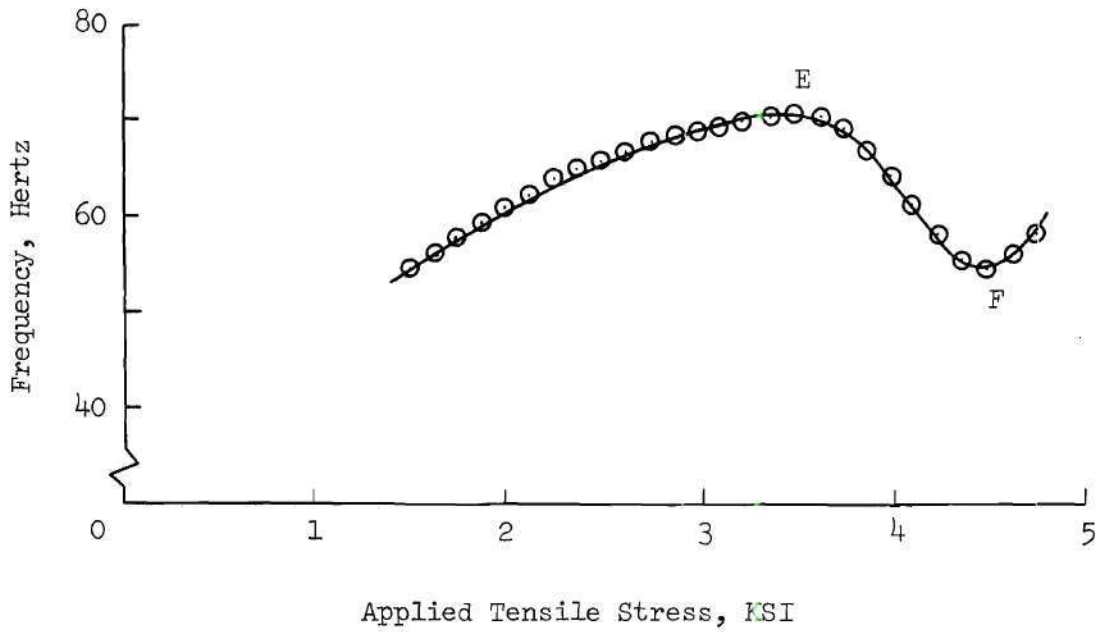

Figure 18(b). Natural Frequency versus Applied Stress Curve for Specimen with Elliptic Hole

included in the experimental investigations because the frequency versus load curve differed substantially from the one obtained for the specimen with the circular hole.

Strictly speaking, the loading on the specimen boundary was not constant. The total load was composed of the mean load and the varying load produced by the shaker. However, the amplitude of the varying load was always kept below one percent of the amplitude of the mean load. This meant, that for all practical purposes, the loading could be considered to have a constant value in the experiment. The total load on the specimen was never allowed to exceed the value of loading which would cause inelastic deformation.

Procedure and Results of Dynamic Stability Investigations

Experiments were also conducted to determine the vibration characteristics of the previously described specimens for an applied dynamic tensile load. The following paragraph describes the procedure used and the data obtained.

After each specimen was placed in the testing fixture a mean load was applied by turning the screw at the top of the fixture. The mean load was measured in the same manner as described in the natural frequency experiments (gages located at point G on the specimen in Figure 20). The electrodynamic shaker was then connected to the horizontal spring. The shaker generated the varying portion of the total load shown in Figure 19. An estimate of the varying load was measured by an oscilloscope. The signal from back to back strain gages (gages located at point H on the specimen in Figure 20) was fed into a

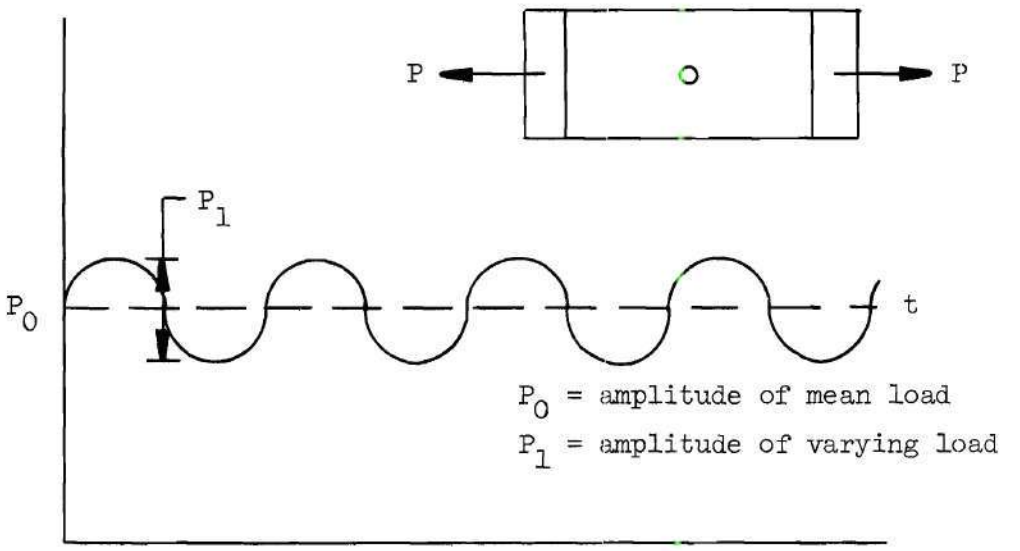

Figure 19. Total Applied Load

bridge which measured the sum of the gage outputs. The output from the bridge was amplified and fed into a calibrated oscilloscope. A schematic diagram of the test facility is shown in Figure 20. A description of the instruments that were used in these experiments is presented in Table 5.

The dynamic bending response of the plate was measured at points I and J in Figure 20. Back to back strain gages at these locations were connected to a bridge which measured the difference in the gage outputs. The signal from the bridge was amplified and fed into a tracking filter. The tracking filter was used to remove all extraneous signals from the system. An external oscillator generated the tuning input to the filter. The output from the filter was fed into a root-

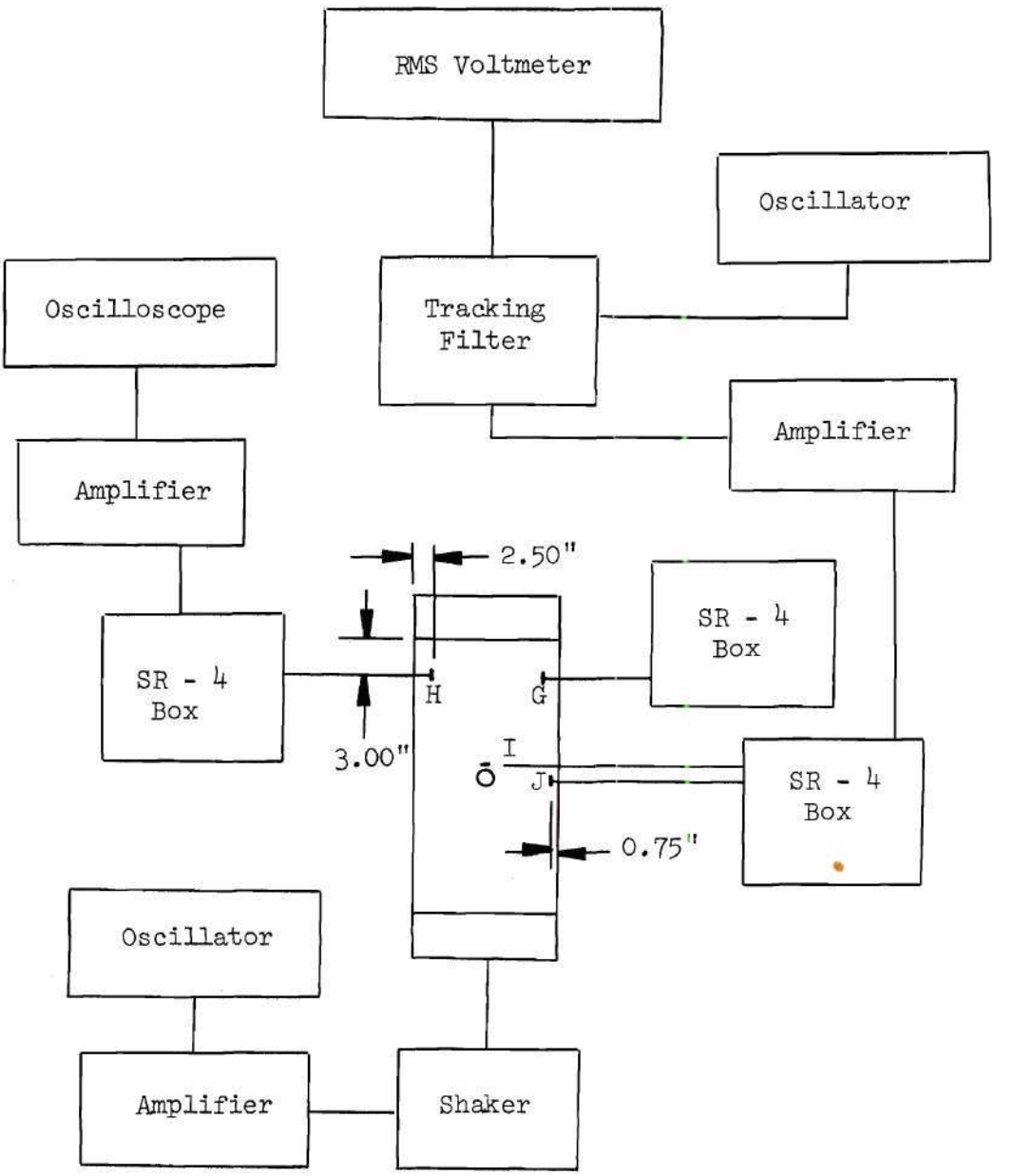

Figure 20. Schematic Diagram for Dynamic Stability Experiment

mean-square voltmeter.

The natural frequency for a given mean load was fed into the tracking filter by the oscillator connected to the filter. The frequency on the oscillator that generated the signal for the shaker was then varied and the responses of the plate at points I and J were recorded by taking readings on the root-mean-square voltmeter.

Typical frequency-response curves are presented in Figure 21 for point I on the specimens. Both specimens exhibited a response at the openings in the plates when the ratio of the natural frequency to the excitation frequency had integer values of one through five. The frequency corresponding to the integer values greater than one were investigated to determine if they were other natural frequencies of the plate. No response from the plate was observed on the voltmeter when both oscillators were set on these frequencies. Therefore, it was concluded that the frequencies where not natural frequencies of the plate. At point J on the specimens only the natural frequencies registered a response on the voltmeter. However, the signals from point J were not as large as the signals at the same frequencies from point I. This tends to indicate the largest response of the specimens is confined to the local regions near the openings in the specimens.

The regions of stable and unstable behavior at the edge of the holes in the specimens can be determined by observing the frequency-response curves at different values of the mean applied load. A plot of these regions is presented in Figures 22(a) and 22(b).

The maximum force rating on the shaker that was used in the experimental investigation was plus or minus 50 pounds. The tensile

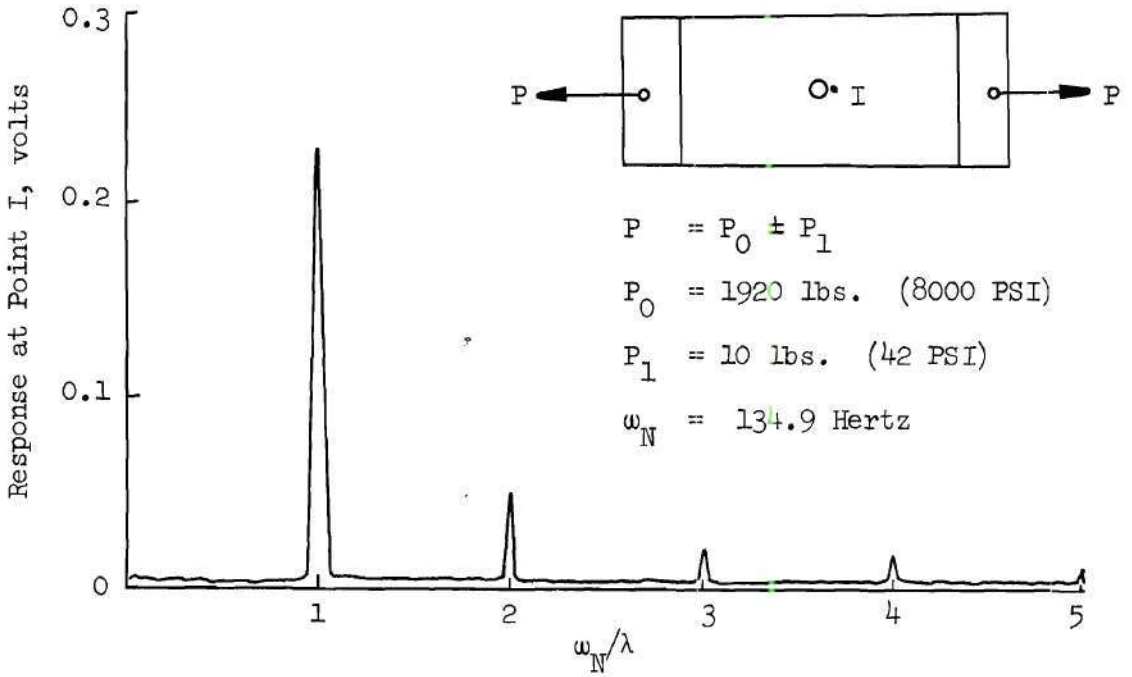

Figure 21(a). Typical Frequency-Response Curve for Specimen Containing Circular Hole

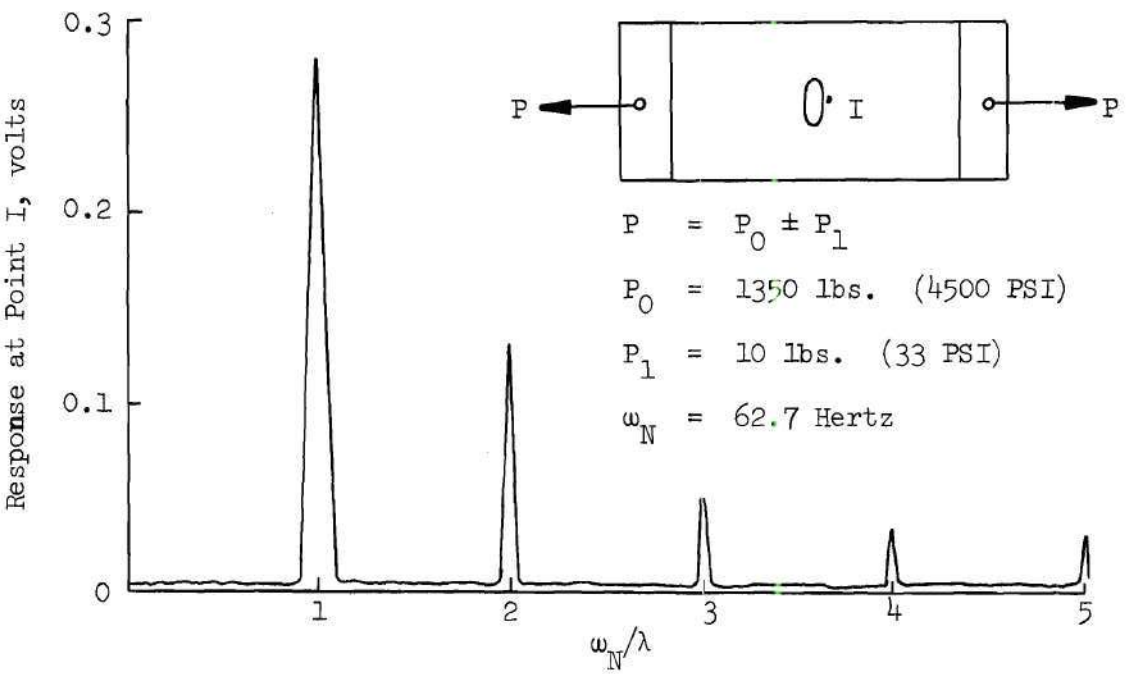

Figure 21(b). Typical Frequency-Response Curve for Specimen Containing Elliptic Hole

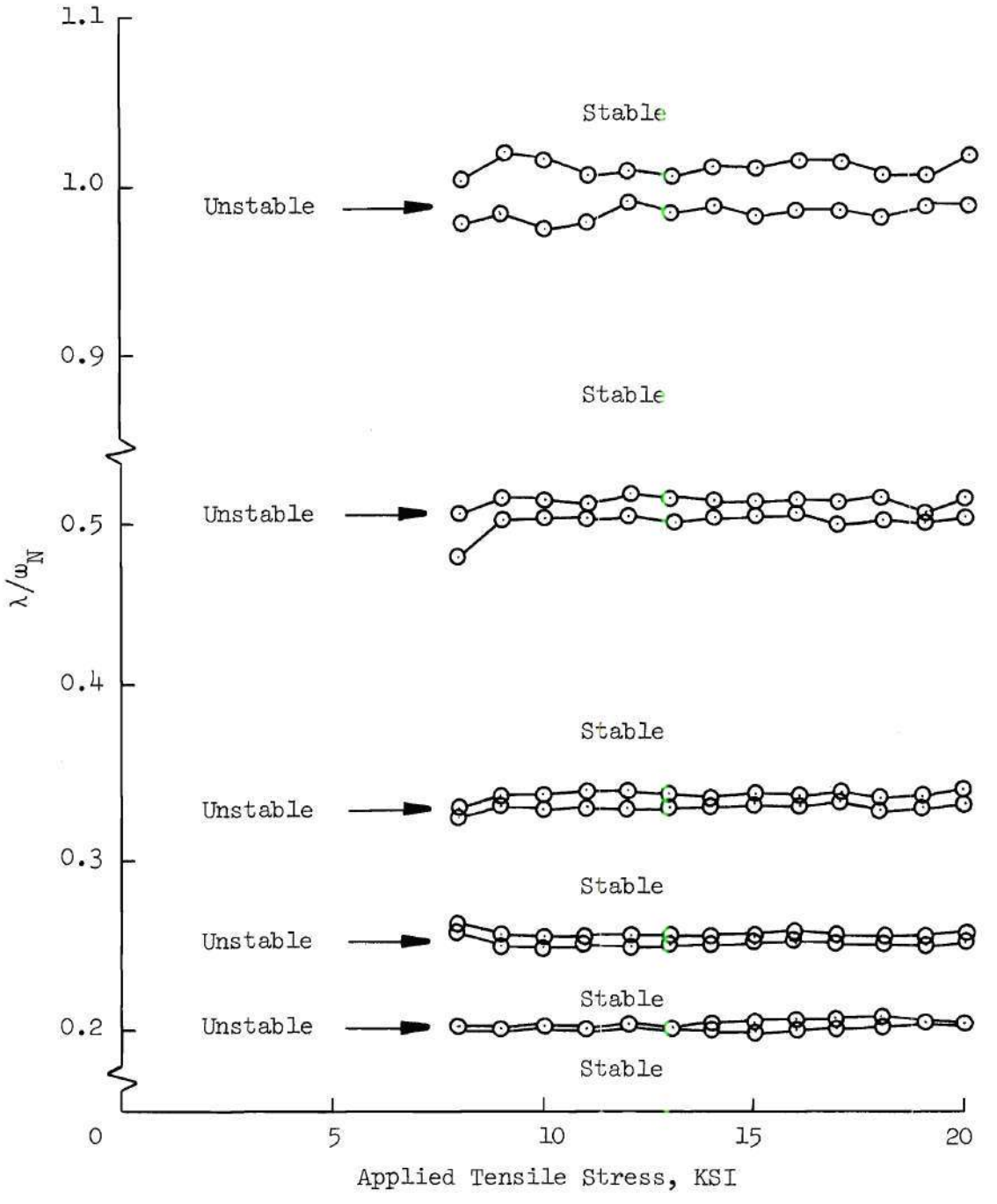

Figure 22(a). Instability Regions for Specimen with Circular Hole

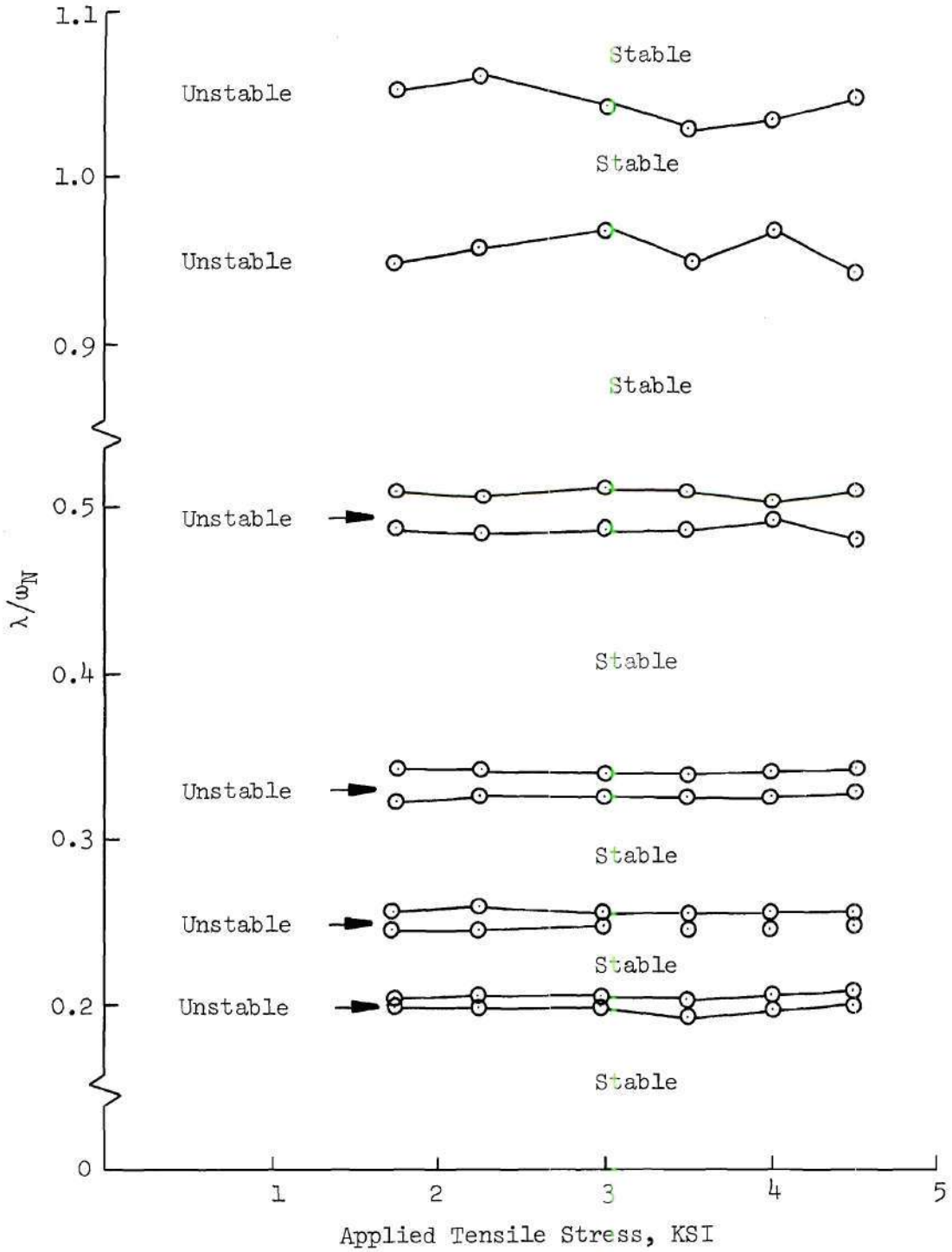

Figure 22(b). Instability Regions for Specimen with Elliptic Hole

buckling loads for the specimens are greater than 1000 pounds. Therefore, the amplitude of the varying load P_1 was limited to a maximum value of less than five percent of the critical load.

The relationship between natural frequency and excitation frequency for the two specimens tested does not compare completely with the frequency relationship found in the dynamic stability investigations of other structural elements [6]. For a small value of the varying load, the frequency ratios of natural frequency to excitation frequency for a column or a plate without an opening when loaded by compressive forces are 1/2, 1, 3/2, 2, 5/2, 3, etc. (see the last section in Chapter III). The frequency ratios for the two plates with centrally located openings are 1, 2, 3, etc. No response was exhibited by the specimens containing holes at the frequency ratios 1/2, 3/2, 5/2, etc.

The theoretical implications of the behavior observed are of considerable interest. The boundary curves which separate stable regions from unstable regions are generated by solutions to the governing differential equation which are periodic with period T and 2T (see last section in Chapter III). These solutions are obtained by solving two independent eigenvalue problems; one for solutions of period T and the other for solutions of period 2T. The frequency ratios of 1, 2, 3, etc. are associated with the solutions of period T and the frequency ratios of 1/2, 3/2, 5/2, etc. are associated with the solutions of period 2T. The absence of responses corresponding to solutions of period 2T implies that the associated eigenvalue problem has only trival solutions. The presence of responses corresponding to solutions of period T implies that non-trival solutions exist for the

associated problem.

It is not possible at present to specify precisely which features of the experimental model cause the observed response to be different from that which is customarily expected in dynamic stability problems. Some discussion of these matters is, however, possible.

The models tested involved a non-uniform stress state which is statically indeterminate. The example problems presented in Reference [6] predominantly involve either uniform stress states or statically determinate stress states. This difference in itself, however, does not necessarily give rise to the observed behavior. It merely causes the problem to be more difficult to analyze.

The natural frequency of the structural element being investigated is an important factor in dynamic stability investigations. In previous investigations in dynamic stability the applied loads have been compressive in nature and this causes the natural frequency versus applied load curves to have a similar characteristic. Namely, the natural frequency decreases continuously with increasing applied load and there is a load axis intercept at the critical value of load. The natural frequency versus applied load curves (Figure 18) for the two specimens that were investigated do not indicate this type of behavior.

In problems of the type described in Reference [6] the eigenfunctions for the associated vibration and buckling problems are either the same or at least similar in form. For the tests described here, the forms of the vibration mode and the buckling mode were quite different. The buckling mode tended to be local and was confined to a

region above and below the holes. The vibration modes were global in character and involved motion of the entire plate.

When the vibration modes and buckling modes are identical, Equations (43) of Chapter II uncouple and it proves convenient in dynamic stability analysies to introduce the ratio

$$\zeta = \frac{P_1}{2(P_{cr} - P_o)} \quad ,$$

where P_{cr} is the critical load. In fact, the frequency ratio ω_N/λ versus ζ plots are often presented to display the regions of stability and instability.

An examination of the above ratio reveals that an infinite number of combinations of P_1 and P_o can be selected to give the same value of ζ. In other words the dynamic stability behavior plot can be established for all load combination possibilities.

In view of the marked difference in the forms of the static and vibration modes for the problems described here, it is not possible to develop fully the dynamic stability behavior by holding P_1 constant and varying P_o. Since the value of P_1 in the present investigation was necessarily small, it follows that the dynamic behavior for large values of P_1 remains unknown for the present.

In view of the substantial differences cited between the specimens tested and the more conventional specimens, it seems reasonable to expect that the details of the dynamic stability response might differ. A detailed explanation of the theoretical significance of these differences must, however, await a more comprehensive investigation.

CHAPTER V

CONCLUSIONS

The problem of local buckling around a circular opening in a large rectangular plate was examined. The loading on the plate was uniform tension on two opposite boundaries. Since the buckling phenomenon was in a local region adjacent to the circular hole, the outer rectangular boundary was replaced by a circular boundary located at infinity. The expression for the critical load was determined to be:

$$N_{cr} = K_L^1 D/a^2$$

where D is the bending stiffness, a is the hole radius and K_L^1 is the lowest positive eigenvalue in the problem. A previous investigator had determined the value of K_L^1 to be 18.72. Several different approximation series were used in a Galerkin solution procedure to obtain values of K_L^1. All the results obtained indicate that the correct value of K_L^1 should be approximately twice the value obtained by the previous investigator.

The natural vibration of a large circular plate with a circular hole was also investigated. The loading on the boundary was the same as in the static stability problem. The local buckling load was obtained in the vibration problem by finding the smallest value of the tensile boundary loading which made the natural frequency of the plate zero.

As the radius of the outer boundary was increased, values of K_L^1 were obtained. These results were compatible with the previous static stability results and they indicate that if the outer to inner boundary ratio is 50 or larger then the value of K_L^1 does not change.

An experimental investigation was conducted to determine the vibration behavior of two rectangular sheet specimens containing different shaped holes. One specimen had a centrally located circular hole and the other had a centrally located elliptic hole. The first part of the experiment was concerned with finding the natural frequency of each specimen for different values of applied tensile load. The natural frequency of the specimen with a circular hole increased with increasing load. The local region of compressive stress appeared to have little influence on the natural frequency.

There were three distinct regions to the natural frequency versus applied load curve for the specimen with the elliptic hole. Starting from zero load on the specimen, the natural frequency increased with increasing applied load. When the applied load reached a certain value, the compressive zone adjacent to the hole started to have an influence on the sheet response. The natural frequency then decreased with increasing load. At about the value of the tensile buckling load of the specimen, the natural frequency again begin to increase as the load continued to increase. The local tensile buckling loads could not be obtained from the natural frequency versus applied load curves because the curves never intersected the applied load axis. The presence of specimen imperfection and middle surface stretching due to bending are believed to be responsible for this behavior.

The second part of the experiment was concerned with determining the vibration characteristics of the previously described specimens for a cyclic tensile load. The dynamic bending response of the plate was measured at the lip of the holes in the specimens. A response characteristic of the type normally encountered in dynamic stability is observed when the ratio of the specimen's natural frequency to the excitation frequency is equal to the integer values of 1, 2, 3, etc. This frequency relationship does not compare completely with the ones found in the dynamic stability investigations of other structural elements. A discussion of the theoretical implications of this response was presented. It is suggested that additional studies be conducted in which the varying component of the total load is larger than that which was possible in the test facility used.

CHAPTER VI

RECOMMENDATIONS FOR FUTURE RESEARCH

The static and dynamic behavior of several plates containing centrally located openings has been described in this manuscript. The results obtained could be more completely explained and further insight into the problem could be developed through extensions of the present research.

It was found that there are frequencies below the lowest natural frequency of the plate at which a resonant type behavior was observed in the region adjacent to the opening in the plate. A more extensive experimental investigation should be conducted in order to obtain more information about this type of behavior. A better understanding of how larger values of the varying load affects the vibration characteristics of the plate should be obtained. Plates with other hole shapes should also be investigated. For example, a plate containing a centrally located crack should be investigated. If there are frequencies below the lowest natural frequency that cause a resonant type behavior in a plate containing a crack, then an investigation should be conducted in order to determine what effect this behavior has on crack propagation rates.

An approximate value of the local tensile buckling load of an infinite plate containing a circular opening was found by using a Galerkin solution procedure. A more exact value of the buckling load

should be obtained. One suggestion would be to investigate other approximation functions in order to achieve more rapid convergence to the exact solution. Another suggestion would be to use a different solution procedure, perhaps finite difference or finite element. Once a more exact value of the buckling load is obtained, a theoretical investigation of the dynamic stability problem should be conducted. This should contribute to a better understanding of the experimental results that were obtained in this research work.

APPENDIX A

IDENTITIES USED IN DERIVING STRAIN-DISPLACEMENT EQUATIONS

$$\vec{g}_1 \cdot \frac{\partial \vec{g}_1}{\partial \alpha_1} = G_1 \frac{\partial G_1}{\partial \alpha_1}$$

$$\vec{g}_1 \cdot \frac{\partial \vec{g}_2}{\partial \alpha_1} = G_1 \frac{\partial G_1}{\partial \alpha_2}$$

$$\vec{g}_1 \cdot \frac{\partial \vec{g}_1}{\partial \alpha_2} = G_1 \frac{\partial G_1}{\partial \alpha_2}$$

$$\vec{g}_1 \cdot \frac{\partial \vec{g}_2}{\partial \alpha_2} = - G_2 \frac{\partial G_2}{\partial \alpha_1}$$

$$\vec{g}_2 \cdot \frac{\partial \vec{g}_1}{\partial \alpha_1} = - G_1 \frac{\partial G_1}{\partial \alpha_2}$$

$$\vec{g}_2 \cdot \frac{\partial \vec{g}_2}{\partial \alpha_1} = G_2 \frac{\partial G_2}{\partial \alpha_1}$$

$$\vec{g}_2 \cdot \frac{\partial \vec{g}_1}{\partial \alpha_2} = G_2 \frac{\partial G_2}{\partial \alpha_1}$$

$$\vec{g}_2 \cdot \frac{\partial \vec{g}_2}{\partial \alpha_2} = G_2 \frac{\partial G_2}{\partial \alpha_2}$$

These identities were obtained by a derivation similar to the one presented in Reference [27].

APPENDIX B

TRANSFORMATION FROM THE GENERALIZED EIGENVALUE PROBLEM TO THE SPECIAL EIGENVALUE PROBLEM

Consider the eigenvalue problem of the form

$$\left[A\right]\left\{x\right\} = \mu \left[B\right]\left\{x\right\} , \tag{B-1}$$

where $\left[A\right]$ and $\left[B\right]$ are real symmetric square matrices, $\left\{x\right\}$ is a column matrix of unknown coefficients and μ is a parameter. The problem involves finding values of μ for which non-trivial solutions exist to the homogeneous set of equations. The problem as given by the matrix equation above is called a generalized eigenvalue problem. If the B matrix is equal to the identity matrix I (the identity matrix has the diagonal elements equal to unity and the off-diagonal elements equal to zero), Equation (B-1) becomes

$$\left[A\right]\left\{x\right\} = \mu \left[I\right]\left\{x\right\} . \tag{B-2}$$

In order to use the Jacobi method to obtain eigenvalues and eigenvectors, the matrix Equation (B-1) must be reduced to the form in Equation (B-2).

The matrix $\left[B\right]$ in Equation (B-1) can be expressed in the form

$$[B] = [Q][D][Q]^T,$$

where $[D]$ is a diagonal matrix of the eigenvalues of the B matrix and $[Q]$ is a matrix of the eigenvectors of the B matrix. A transformation of the form $[Q][D][Q]^T$ is called a similarity transformation. Substituting this expression for $[B]$ into Equation (B-1) gives

$$[A]\{x\} = \mu [Q][D][Q]^T \{x\} .$$

Since the D matrix is diagonal, this equation can be written as

$$[A]\{x\} = \mu [Q][D^*][D^*][Q]^T \{x\} , \qquad \text{(B-3)}$$

where the matrix D^* is obtained by taking the square root of the elements in the D matrix. Pre-multiplying Equations (B-3) by the inverse of the matrix product $[Q][D^*]$ and using the fact that the inverse of a matrix product is equivalent to the inverse of the individual matrices in reverse order, yields the equation

$$[D^*]^{-1}[Q]^{-1}[A]\{x\} = \mu [D^*][Q]^T \{x\} .$$

Post-multiplying $[A]$ and $[Q]^{-T}$ in the above equation by the identity matrix formed by the product of $[D^*][Q]^T$ and its inverse, the following equation is obtained:

$$\left[C\right]\left\{y\right\} = \mu\left[I\right]\left\{y\right\}, \tag{B-4}$$

where $$\left[C\right] = \left[D^*\right]^{-1}\left[Q\right]^{-1}\left[A\right]\left[Q\right]^{T^{-1}}\left[D^*\right]^{-1}$$

and $$\left\{y\right\} = \left[D^*\right]\left[Q\right]^{T}\left\{x\right\} .$$

If the eigenvectors of the Q matrix are normalized so that they are unit vectors, the inverse of the Q matrix is equal to the transpose of the Q matrix [28] and the C matrix can be written as

$$\left[C\right] = \left[D^*\right]^{-1}\left[Q\right]^{T}\left[A\right]\left[Q\right]\left[D^*\right]^{-1} .$$

The Jacobi method can now be used to obtain the eigenvalues and eigenvectors of the homogeneous system of equations given by Equation (B-4).

The transformation from the generalized problem to the special problem does not change the value of the eigenvalues. However, the eigenvectors are changed. The eigenvectors are related by the equation

$$\left\{y\right\} = \left[D^*\right]\left[Q\right]^{T}\left\{x\right\} .$$

APPENDIX C

METHOD OF SOLVING GENERALIZED EIGENVALUE PROBLEM

A method for finding eigenvalues of the homogeneous equations

$$\left[A\right]\left\{x\right\} = \mu\left[B\right]\left\{x\right\} \tag{C-1}$$

is presented in this appendix. The eigenvalues of this system of equations are the values of μ for which the determinant $\Delta(\mu)$, defined as

$$\Delta(\mu) = \left| \left[A\right] - \mu\left[B\right] \right| ,$$

is equal to zero. For an assumed value of μ, the determinant $\Delta(\mu)$ can be calculated. A plot of $\Delta(\mu)$ versus μ can then be made by successively picking values of μ and calculating corresponding values of the determinant. The values of μ at which the curve intersects the μ axis are the eigenvalues of Equations (C-1).

In order to calculate an eigenvalue accurately, the method described above was used in conjunction with an iteration routine. Once a change in sign of $\Delta(\mu)$ was located, an iteration routine was used to converge to the value of μ for which $\Delta(\mu)$ was equal to zero.

APPENDIX D

VALUES OF THE EXPONENTIAL INTEGRALS

$$E(m) = e^{m} \int_{1}^{\infty} \frac{1}{r} e^{-mr} \, dr$$

$E(2) = .3613286$

$E(3) = .2620837$

$E(4) = .2063457$

$E(5) = .1704222$

$E(6) = .1452676$

$E(7) = .1266411$

$E(8) = .1122796$

$E(9) = .1008620$

$E(10) = .0915633$

$E(11) = .0838418$

$E(12) = .0773261$

$E(13) = .0717535$

$E(14) = .0669325$

These values were obtained from Reference [29].

APPENDIX E

TRIGONOMETRIC IDENTIES

$n = 1,2,3,\ldots$ and $\ell = 1,2,3, \ldots$

$$\int_0^{2\pi} \cos n\theta \cos \ell\theta \, d\theta = \begin{cases} \pi ; & n = \ell \\ 0 ; & n \neq \ell \end{cases}$$

$$\int_0^{2\pi} \cos 2\theta \cos n\theta \cos \ell\theta \, d\theta = \begin{cases} \pi/2 ; & \ell = n + 2 \\ \pi/2 ; & n = \ell + 2, \; n = \ell = 1 \\ 0 ; & \text{otherwise} \end{cases}$$

$$\int_0^{2\pi} \sin 2\theta \sin n\theta \cos \ell\theta \, d\theta = \begin{cases} -\pi/2 ; & \ell = n + 2 \\ \pi/2 ; & n = \ell + 2, \; n = \ell = 1 \\ 0 ; & \text{otherwise} \end{cases}$$

REFERENCES

1. Panovko, Y. G. and Gubanova, I. I., Stability and Oscillations of Elastic Systems, (Translated by C. V. Larrick) Consultants Bureau, New York, N. Y., 1965, p. 7.

2. Beliaev, N. M., "Stability of Prismatic Rods Subjected to Variable Longitudinal Forces," Engineering Constructions and Structural Mechanics, Leningrad, Russia, 1924, p. 149.

3. Einaudi, R., "About Unstable Equilibrium States of Plates Subject to Periodic Shear Stresses," Atti Accad. Gioenia, Memoria XX, 1935, p. 1.

4. Chelomei, V. N., "Dynamic Stability of Plates," Tr. Kiev. Aviats. Inst., No. 10, 1938.

5. Bodner, V. A., "Stability of Plates Subjected to Longitudinal Periodic Forces," Prikladnia Melematika Mekhanika, Vol. 2, No. 1, 1938, p. 87.

6. Bolotin, V. V., "The Dynamic Stability of Elastic Systems," Holden-Day, San Francisco, California, 1964.

7. Somerset, J. H. and Evan-Iwanowski, R. M., "Influence of Non-Linear Inertia on the Parametric Response of Rectangular Plates," International Journal of Non-Linear Mechanics, Vol. 2, Sept. 1967, p. 217.

8. Somerset, J. H. and Evan-Iwanowski, R. M., "Experiments on Large Amplitude Parametric Vibration of Rectangular Plates," Developments in Theoretical and Applied Mechanics, Vol. 3, Shaw, W. A. (ed). Pergamon Press, London, England, 1967, p. 331.

9. Willems, N. and Duffield, R. C., "Parametric Stability of Rectangular Plates Reinforced with Closely Spaced Stiffners," Developments in Mechanics, Vol. 5, Iowa State University Press, Ames, Iowa, 1969, p. 387.

10. Beilin, E. A. and Dzhanelidze, G. U., "Survey of Work on the Dynamic Stability of Elastic Systems," Prikl, Mat, i Mekhan., Vol. 16, No. 5, p. 635, (Available in English as ASTIA No. AD-264148).

11. Evan-Iwanoski, R. M., "On the Parametric Response of Structures," Applied Mechanics Review, Vol. 18, No. 9, Sept. 1965, p. 699.

12. Kraus, H., Thin Elastic Shells, Wiley and Sons, Inc., New York, N. Y., 1967, p. 47.

13. Bolotin, V. V., loc. cit. Ref. 6, p. 111.

14. Somerset, J. H. and Evan-Iwanowski, R. M., loc. cit. Ref. 8, p. 331.

15. Neuber, H., Theory of Notch Stresses: Principles for Exact Stress Calculation, DTMB Translation, No. 74, 1945, p. 36.

16. Goldenveizer, A. L., Theory of Elastic Thin Shells, International Series of Monographs in Aeronautics and Astronautics, Translated by G. Herrmann, Pergamon Press, New York, N. Y., 1961, p. 59.

17. Timoshenko, S. P. and Goodier, J. N., Theory of Elasticity, McGraw-Hill Book Co., New York, N.Y., 1961, p. 78.

18. Pellett, D. A., "Buckling Near a Hole in a Infinite Plate," Dissertation, Naval Postgraduate School, Monterey, Calif., 1967.

19. Timoshenko, S. P. and Gere, J. M., Theory of Elastic Stability, McGraw-Hill Book Co., New York, N. Y., 1961, p. 348.

20. Ralston, A., A First Course in Numerical Analysis, McGraw-Hill Book Co., New York, N. Y., 1965, p. 487.

21. Costello, R. G., "Buckling Near a Hole in a Infinite Plate," Dissertation, Naval Postgraduate School, Monterey, Calif., 1968.

22. Datta, P. K., "On the Buckling and Vibration Behavior of a Thin Tensioned Sheet with an Elliptical Hole," Doctoral Dissertation, Georgia Institute of Technology, Atlanta, Georgia, 1972.

23. Mikhlin, S. G., Approximate Methods for the Solution of Differential and Integral Equations, American Elsevier Co., New York, N. Y., 1967, p. 229.

24. Bisplinghoff, R. L., Ashley, H. and Halfman, R. L., Aeroelasticity, Addison-Wesley Co., Reading, Mass., 1957, p. 165.

25. Bolotin, V. V., loc. cit. Ref. 6, p. 19.

26. Bolotin, V. V., loc. cit. Ref. 6, p. 220.

27. Washizu, K., Variational Methods in Elasticity and Plasticity, Pergamon Press, New York, N. Y., 1968, p. 76.

28. Hildebrand, F. B., Methods of Applied Mathematics, Prentice-Hall, Englewood Cliffs, N. J., 1952, p. 38.

29. Pagurova, V. I., Tables of Exponential Integrals, Pergamon Press, New York, N. Y., 1961.

30. Fung, Y. C., Foundations of Solid Mechanics, Prentice-Hall, Englewood Cliffs, N. J., 1965.

31. Pellett, D. A., Costello, R. G. and Brock, J. E., "Buckling of a Tension Panel Containing a Circular Hole," AIAA Journal, Vol. 6, No. 10, October 1968, p. 2012.

32. Zielsdorff, G. F., "An Investigation of the Out-of-Plane Deflection Behavior of Thin Sheets with Cut-outs in a Tensile Field", Doctoral Dissertation, Georgia Institute of Technology, Atlanta, Georgia, 1971.

VITA

Guerry C. Backer was born April 11, 1943 in Macon, Georgia. He attended grammar school in Macon and graduated from Lanier High School in 1961.

Mr. Backer became a student at the Georgia Institute of Technology in September 1961 and graduated in December 1965 with a Bachelor's degree in aerospace engineering. He was a member of Sigma Alpha Epsilon social fraternity.

Upon graduating from Georgia Tech Mr. Backer worked for the Lockheed-Georgia Company. He received the Technical Excellence Award while at Lockheed for his work on the C-5A ailerons. While working at Lockheed, Mr. Backer, also attended Georgia Tech on a part time basis. He received an M. S. in A.E. in June of 1970. Shortly after receiving this degree Mr. Backer left Lockheed to devote full time to graduate work at Georgia Tech. He was awarded a Lockheed Leadership Fellowship during this period.

He is married to the former Lynn Cobb of Houston, Texas. They have a daughter and presently reside in Pascagoula, Mississippi.